

TECHNICAL CONSIDERATIONS FOR ^1H - MAGNETIC RESONANCE
SPECTROSCOPY (^1H -MRS) MEASUREMENT OF SPINAL CORD
GAMMA-AMINOBUTYRIC ACID (GABA)

TECHNICAL CONSIDERATIONS FOR ^1H - MAGNETIC RESONANCE
SPECTROSCOPY (MRS) MEASUREMENT OF SPINAL CORD
GAMMA-AMINOBUTYRIC ACID (GABA)

By Nicholas SIMARD,

*A Thesis Submitted to the School of Graduate Studies in the Partial Fulfillment
of the Requirements for the Degree Master's of Applied Science*

McMaster University © Copyright by Nicholas SIMARD January 4, 2019

McMaster University

Master's of Applied Science (2019)

Hamilton, Ontario (School of Biomedical Engineering)

TITLE: Technical Considerations for ^1H - Magnetic Resonance Spectroscopy (MRS)
Measurement of Spinal Cord gamma-aminobutyric acid (GABA)

AUTHOR: Nicholas SIMARD (McMaster University)

SUPERVISOR: Dr. Michael D. NOSEWORTHY and Dr. Aimee NELSON

NUMBER OF PAGES: xiii, 76

Lay Abstract

The spinal cord is an area often overlooked in science and in medicine. A new investigative tool is required to understand how contents of the in-vivo spinal cord interact in certain pathological settings. Using an MRI should therefore be investigated, specifically a technique termed MRS, to collect data on the contents of an area of interest within the spinal cord. After acquiring repeatedly poor data, new techniques were examined to help improve data quality. First, to ensure the MRS technique is working, data from a control phantom was analyzed. This phantom allows for calibration of the MRS technique and ensures that data is being collected properly. However, when MRS is attempted in the human spinal cord, poor data is continually collected. Therefore, noise reduction and signal boosting techniques were implemented to a certain degree of success for future MRS spinal cord applications. The results suggest that a lot of work needs to be done to improve the MRS technique for spinal cord applications, however, one day this method can be clinically relevant and help us understand the secrets that lie within the spinal cord.

Abstract

Neurometabolites in the spinal cord play a significant role in biomechanics and neural plasticity. However, due to low concentrations and the limited geometry of the spinal cord, neurometabolites are not investigated with imaging modalities or in vivo. Therefore, the goal of this ^1H -Magnetic Resonance Spectroscopy (^1H -MRS) research was to assess a variety of techniques that aim to improve collection and quantification of in-vivo neurometabolite data in the cervical spinal cord using a Magnetic Resonance Imaging (MRI) scanner. This is important as the cervical spine can reveal information on the upper limb and its neuronal innervation nature. In this research, a phantom study was introduced as a proof of concept to ensure data acquisition based on spinal geometry can be repeatable and accurate. T-tests were performed to identify if ^1H -MRS analysis was accurate and significant ($P < 0.05$). MR spectral fit quality was assessed using two MRS fitting software packages (LCmodel and Tarquin) to see which more appropriately fit the data, based on standard and known concentrations in phantoms. T-test results found that both software packages can significantly ($P < 0.05$) provide useful information on the spinal cord content concentrations, although software packages use different estimation methods. Furthermore, physiological motion such as breathing and pulsatile flow in the vessels that surround and flow through the spinal cord (i.e. CSF, blood) contribute to the highest levels of noise in the MRS signal. Therefore, a study that included the investigation of main magnetic field (B_0) and RF transmit field (B_1^+) inhomogeneities was conducted to evaluate how physiological noise (Pulsatile flow (PPG) and Respiratory flow (RESP) data) affects data quality. Research found that there exists a relationship between PPG data and the B_0 field (Correlation of 0.71) whereas RESP data and the B_1^+ field also yielded a relationship (Correlation of 0.62). Additional noise reduction techniques were also investigated to determine further improvement in spinal cord MRS data acquisition to best understand neurometabolite behaviour in this challenging tissue.

Dedication and Acknowledgements

I would truly like to thank my supervisors, Dr. Michael Noseworthy and Dr. Aimee Nelson, for the opportunity to work in their labs and for all of their guidance and support provided over these past two years. Norm Konyer thank you for all of your help, especially on the technical side of things and to Diana Harasym for working alongside similar project objectives. Further, I would like to acknowledge the IRC technologists, Carol Awde, Cheryl Conant, and Julie Lecomte, for all the work during the data collection stages.

And last but not least, a huge thank you to all my labmates; Alireza Akbari, Michael Behr, Caty Charles Herrera, Olga Dona Lemus, Mitch Doughty, Jenin El-Sayes, Hunter Fassett, Diana Harasym, Amy Harrison, Mitch Locke, Evan McNabb, Conrad Rockel, Alejandro Santos Diaz, Mitch Savoie, Saurabh Shaw, Stephen Toepp, and Claudia Turco. It's been an absolute pleasure getting to know each and every one of you. Thanks everyone for a great two years! . . .

Contents

Lay Abstract	iii
Abstract	iv
Dedication and Acknowledgements	v
Abbreviations	xi
Declaration of Authorship	xiii
1 Introduction	1
1.1 Thesis Statement	1
1.2 Proposed Solution	2
1.2.1 Objectives	3
1.2.2 Hypothesis	4
1.3 Significance of Research	5
1.4 Outline of Thesis Chapters	6
2 Background and Literature Review	7
2.1 MRI Overview	7
2.1.1 ¹ H-Magnetic Resonance Spectroscopy (¹ H-MRS)	8
2.1.2 Cervical Spinal Cord Imaging	11
2.1.3 B ₀ and B ₁ ⁺ Measurements	13
2.2 Gamma-Aminobutyric Acid (GABA)	17

3	¹H-Magnetic Resonance Spectroscopy Phantom Study	22
3.1	Rationale	22
3.2	Hypotheses	23
3.3	Methods	23
3.3.1	Phantom Device	23
3.3.2	¹ H-MRS Sequences and Protocols	25
3.3.3	Analysis Pipeline	27
3.4	Results and Discussion	28
3.4.1	LCModel analysis of the PRESS sequence	28
3.4.2	LCModel analysis of the MEGA-PRESS sequence	31
4	Comparison of ¹H-MRS Software Tools	36
4.1	Rationale	36
4.2	Hypotheses	37
4.3	Methods	38
4.3.1	Phantom Device	38
4.3.2	¹ H-MRS Sequences and Protocols	38
4.3.3	Analysis Pipeline	38
4.4	Results and Discussion	40
4.4.1	TARQUIN analysis of the PRESS sequence	40
4.4.2	TARQUIN analysis of the MEGA-PRESS sequence	43
4.4.3	TARQUIN and LCModel software comparison	47
5	In vivo Measurements of B_0 and B_1^+ Variations as Confounders in ¹H-MRS	49
5.1	Rationale	49
5.2	Hypotheses	50
5.3	Methods	50

5.3.1	Participants	50
5.3.2	¹ H-MRS Sequences and Protocols	51
5.3.3	Analysis Pipeline	53
5.4	Results and Discussion	56
6	Conclusions and Future Work	60
6.1	Summary of Findings	60
6.1.1	Experiment 1	60
6.1.2	Experiment 2	61
6.1.3	Experiment 3	62
6.2	Current Challenges and Future Work	63
A	MATLAB Code	65
B	Bash Script Code	67
C	Publisher Permissions	69

List of Figures

2.1	Typical ^1H -MRS Spectrum at 3T	9
2.2	^1H -MRS Voxel positioning in the spinal cord	13
2.3	B_0 field map in a healthy human at spinal level C4	15
2.4	B_1^+ field map in a healthy human at spinal level C4	17
2.5	^1H -MRS spectrum and isolated GABA resonant peaks	19
2.6	The MEGA-PRESS method and its pulse description	21
3.1	BRAINNO solution contents	24
3.2	A constructed cervical spinal cord phantom	25
3.3	Voxel Positioning in Phantom	26
3.4	PRESS mean estimated metabolite concentrations found using LCModel .	29
3.5	PRESS standard deviations and T-test results found using LCModel . . .	30
3.6	MEGA-PRESS mean estimated metabolite concentrations found using LCModel	33
3.7	MEGA-PRESS standard deviations and T-test results found using LCModel	34
4.1	PRESS mean estimated concentrations found using TARQUIN	41
4.2	PRESS standard deviations and T-test results found using TARQUIN . .	42
4.3	MEGA-PRESS mean estimated concentrations found using TARQUIN . .	45
4.4	MEGA-PRESS standard deviations and T-test results found using TAR- QUIN	46
4.5	TARQUIN vs. LCModel T-test results	47

5.1	Pulsed oximeter and respiratory bellow	52
5.2	Phantom and spinal cord ROI selection in B_0 field maps	54
5.3	Processed PPG and RESP data	55
5.4	PCA Analysis using the ΔB_0 , ΔB_1^+ , PPG, and RESP parameters	57
5.5	Correlation Analysis using the ΔB_0 , ΔB_1^+ , PPG, and RESP parameters	58

Abbreviations

¹H-MRS	¹ H-Magnetic Resonance Spectroscopy
BS	Bloch-Siebert
C1	Cervical Spinal Level 1
C2	Cervical Spinal Level 2
C3	Cervical Spinal Level 3
C4	Cervical Spinal Level 4
C6	Cervical Spinal Level 6
Cho	Choline containing compounds
Cr	Creatine
CSF	Cerebrospinal Fluid
DWI	Diffusion-Weighted Imaging
ECG	Electrocardiographic
FWHM	Full Width Half Maximum
GABA	Gamma-Aminobutyric Acid
GABA-T	Gamma-Aminobutyric Acid Transaminase
GAD	Glutamic Acid Decarboxylase
GE	General Electric

MEGA-PRESS	MESHcher-GARwood Point RESolved Spectroscopy
MR	Magnetic Resonance
MRI	Magnetic Resonance Imaging
NAA	N-Acetylaspartate
OVS	Outer Volume Saturation
PRESS	Point RESolved Spectroscopy
RF	Radiofrequency
SEEP	Signal Enhancement by Extravascular water Protons
SNR	Signal-to-Noise Ratio
T1	Thoracic Spinal Level 1
TE	Echo Time
TMS	Transcranial Magnetic Stimulation

Declaration of Authorship

I, Nicholas SIMARD, declare that this thesis titled, “Technical Considerations for ^1H - Magnetic Resonance Spectroscopy (MRS) Measurement of Spinal Cord gamma-aminobutyric acid (GABA)” and the work presented in it are my own.

Chapter 1

Introduction

1.1 Thesis Statement

The execution of upper motor limb movements are often affected by impairment in significant neurological disorders such as stroke, Alzheimer's, Parkinson's, and many more. Impairment is often characterized by a cortical imbalance in excitatory and inhibitory neural circuits, however, often overlooked is the role of the cervical spinal cord and the effect it has on neural circuitry. Although, many neurological disorders cause cognitive function loss and affect hand and forearm functions, it is unclear whether these symptoms are attributed to imbalances in cortical circuitry or imbalances in spinal cord circuitry (Convento, 2016; Ludemann-Podubecka, 2014). The cervical spinal cord is viewed as this neglected area of study in neuroscience due to the lack of safe and accurate investigation methods (Convento, 2016). Currently, the only reliable method of investigation includes a biopsy which is a highly invasive and slightly dangerous procedure that requires a sample of an individual's spinal cord to complete an assessment (Hock, 2013). Biopsies are performed when MRI studies are inconclusive and help provide pathological information such as the contents of neuro-inflammatory mediators and enzymes (Cohen-Gadol, 2003). The most respected alternative to biopsy includes a highly non-invasive

and safe procedure termed ^1H magnetic resonance spectroscopy (^1H -MRS). ^1H -MRS utilizes the principles of magnetic resonance imaging (MRI) to identify and quantify chemical metabolites in neuronal tissue. The ^1H -MRS tool was first utilized for the investigation of cortical tissue, however presents itself with a variety of technical nuances when translating the technique to a spinal cord setting. Characteristics such as susceptibility differences, motion artifacts, tissue inhomogeneities, and small geometries of interest all have their own negative effects on the quality of data that ^1H -MRS acquires (Henning, 2008). **Therefore, the goal of this Master’s thesis was to advance the existing ^1H -MRS technique to further perform reliable and reproducible in vivo experiments of the human cervical spinal cord.**

1.2 Proposed Solution

Advanced imaging and spectroscopic methods are required to improve the reliability and reproducibility of ^1H -MRS acquisitions in cases of cervical spinal cord investigation. Reproducibility is a primary target of success as it ensures that measurements are precise, however, a reliable baseline is needed to properly assess a reproducibility metric. As the ^1H -MRS technique identifies the biochemical composition of the spinal cord, specific metabolites found within neuronal tissue must be selected as frames of reference. Therefore, metabolites selected for evaluation included N-Acetylaspartate (NAA) and Gamma-Aminobutyric acid (GABA). These metabolites were carefully selected for research as NAA is a primary metabolite within every neuronal tissue and is found in high concentrations (Hashimoto, 1995). Whereas, GABA is a key inhibitory neurotransmitter that often plays a role in pathological and neuroplastic settings (Wolff, 1993). These metabolites are crucial in better understanding the underlying mechanisms of the spinal cord and were therefore the primary targets of current and future investigation.

Technical nuances create a lack of reliability within ^1H -MRS measurements and were therefore thoroughly investigated. Understanding the principles behind issues such as low signal volume, susceptibility differences due to non-homogeneous tissue-tissue boundaries (i.e. between bone, intervertebral discs, neural tissue, fat, muscle, tendon, vasculature, etc.), pulsatile flow in or around the spinal cord, and software analysis inconsistencies should lead to better assessment of accurate measurements (Henning 2008). Investigating each technical issue thus should help understand where artifacts and sources of noise originate and identify possible solutions that can mitigate these sources of error.

The proposed solution towards improving ^1H -MRS in the cervical spinal cord therefore includes the investigation of novel methods for quantifying GABA metabolite concentrations within the human cervical spinal cord. Combining these novel techniques could unlock previously undiscovered neuroscience secrets and help us better understand problems such as stroke, Alzheimer's, and Parkinson's within the context of upper limb pathology.

1.2.1 Objectives

The main objective of this thesis was to develop a reliable ^1H -MRS technique that adequately reduces noise, increases signal, and allows for reproducible and reliable GABA concentration measurements within the cervical spinal cord region (C1 - T1). Through a distinct ^1H -MRS protocol, this research aims to provide further evaluation and information on physiological changes within the spinal cord which occur during neurological diseases such as stroke, Alzheimer's, Parkinson's, and spinal cord injury. The following experiments define specific objectives that focused on achieving the goals of this thesis research.

Experiment 1

The goal of Experiment 1 was to investigate the reliability and reproducibility of measuring GABA in a controlled phantom environment; the phantom replicated the spinal cord geometry and its dominating metabolite contents.

Experiment 2

The goal of Experiment 2 was to investigate the reliability and reproducibility of two software packages (LCModel and TARQUIN). The dominant inhibitory neurotransmitter, GABA, was chosen due to its importance in the central nervous system. Experiment 2 was conducted in a home deign/built MRI spectroscopy phantom.

Experiment 3

The goal of Experiment 3 was first to develop a proposal for spinal cord MRS acquisition. This was a challenge due to the irregular non-orthogonal direction of the cord, with respect to the direction of the main magnetic field B_0 . Once established the goal was to investigate the relationship between a healthy human spinal cord (spinal segments C2-C4) and B_0 and B_1+ MRI parameters. A distinct relationship would provide researchers with a new noise reduction tool to eliminate physiological signals from cervical spinal cord ^1H -MRS measurements. Experiment 3 was conducted in 10 healthy humans.

1.2.2 Hypothesis

The premise of the above experiments provides the overarching goal of this work which was to assess GABA within the human cervical spinal cord using ^1H -MRS.

- A phantom study will ensure that current techniques can be implemented for small cylindrical geometries and provide comparable concentrations of GABA to known concentrations.

- A software comparison was performed to identify whether an open source software package (TARQUIN) provided equally as comparable results, compared to expensive alternative (LCmodel).
- Physiological confounding factors such as blood flow and respiratory motion induce noise within the B_0 and B_1+ MR parameters. Through statistical analysis, a correlation was found that permits better acquisition and data post-processing, therefore benefiting future measurements.

1.3 Significance of Research

The data obtained from this MASc thesis should provide novel ^1H -MRS techniques that improve data collection within the cervical spinal cord. Advances in this domain can unlock a breadth of neuroscientific information for developing clinically relevant biochemical references for the spinal cord's role in neurological disorders (Kakulas, 2015; Cadotte, 2012). An improvement in spinal cord data collection should also offer clinical aid in developing personalized and disease specific treatments for the abundant variety of neurological disorders that affect millions worldwide (Kakulas, 2015; El Masri, 2006). The future aim of these improved ^1H -MRS techniques can also manifest in the investigation of techniques that help quantify the relationship that spinal neuroplasticity shares with rehabilitation. Specifically, the impact and role of the inhibitory neurotransmitter GABA at spinal levels C6-T1 (Cervical 6 - Thoracic 1)(Mescher, 1996; 1998). GABA is the dominant inhibitory neurotransmitter in the brain and spinal cord and is important in motor learning and developing neuroplastic pathways (Blicher, 2004; Wolff, 1993). In addition, the resulting research will help in the future validation of transcranial magnetic stimulation (TMS) approaches as potential therapeutic approaches that can alter

neural output to the hand and forearm muscles (i.e. muscles affected by spinal levels C6-T1)(Convento, 2016; Wolff, 1993).

1.4 Outline of Thesis Chapters

The experiments presented in this thesis were either performed in a constructed phantom or in healthy adults. Chapter 2 includes a review of MRS and its MRI principles along with a review of the literature and methodology pertinent to this Master's thesis. Detailed descriptions of the methods employed, specific hypotheses and results from Experiments 1, 2, and 3 will follow in Chapters 3, 4, and 5, respectively. An overall discussion in Chapter 6 will provide interpretation of the findings from the MASc experiments along with thoughts of future work and personal notes and critiques on the work presented.

Chapter 2

Background and Literature Review

2.1 MRI Overview

MRI is a non-invasive medical imaging technique which uses a static magnetic field, linear magnetic field gradients and radiowave pulses to image anatomy and physiological processes within the human body. Subjects are placed in a large, homogeneous magnetic field, B_0 and the acquired signals are digitized and reconstructed into two-dimensional images. Often the end result is a tomographic series of images. The same principles can also be used to detect a number of important metabolites through the process of magnetic resonance spectroscopy (MRS). Instead of acquiring a typical two-dimensional image, MRS plots the intensities of certain chemicals of interest and can detect the concentration of a number of important neurotransmitters. These plots can therefore identify the specific biochemical composition of areas of interest within the human body unlocking potential physiological information, and providing correlates to anatomy.

2.1.1 ^1H -Magnetic Resonance Spectroscopy (^1H -MRS)

^1H -magnetic resonance spectroscopy (^1H -MRS) is a promising tool that can identify the biochemical nature of specific tissues, including brain tissue (Henning, 2008; Heinzer-Schweizer, 2010; de Graaf, 1998). It has been applied at 1.5T, but due to better spectral resolution and SNR it has now become a method more often done at 3T or higher. ^1H -MRS provides a non-invasive platform that can identify concentrations of metabolites such as N-Acetylaspartate (NAA), Choline containing compounds (Cho), Creatine (Cr), and Gamma-Aminobutyric acid (GABA) (Mullins, 2014). Neuronal metabolites and their concentrations can indicate neuronal density, neuronal dysfunction, neurotransmitter excretions, distorted membrane synthesis, metabolic malfunctions, demyelination, and much more (Henning, 2008). Metabolites and their biochemical information are therefore instrumental in identifying and understanding neuronal tissue behaviour and in-depth research will lead to better understanding of diagnosis, disease progression, treatment planning, and rehabilitation mechanics (Hock, 2013).

In order to better understand the MRS technique and its applications, it is helpful to work through the founding principles of ^1H -MRS. Similar to MRI, ^1H -MRS detects radio frequency (RF) signals from nuclear spins of hydrogen. The hydrogen, or proton, nucleus is the most sensitive nucleus for investigation as it has a high gyromagnetic ratio (42.576MHz/T) and high natural abundance (>99.99%) (de Graaf, 1998). Since nearly all metabolites contain hydrogen, ^1H -MRS is a powerful technique to identify, observe, and quantify biologically important compounds found within the human body and spinal cord (de Graaf, 1998). Within each hydrogen nuclear spin signal acquired, there is also an accompanying frequency characteristic which is influenced by the surrounding molecular environment. Therefore each hydrogen nucleus possesses a discrete chemical frequency signature dependent on the other nuclei that surround it. This helps ^1H -MRS signal acquisitions represent chemical-specific frequencies of hydrogen spins within an easy to

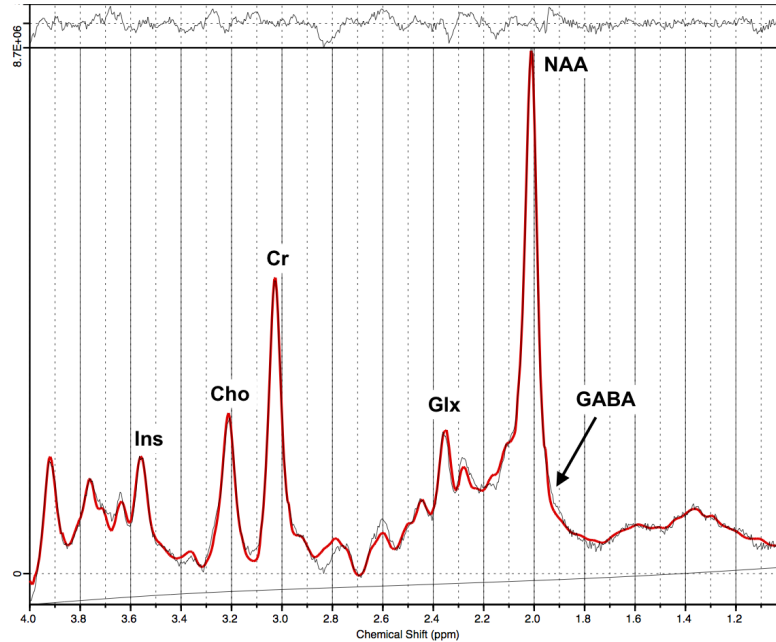


FIGURE 2.1: Typical ^1H -MRS spectrum at 3T of neuronal tissue showing peaks of certain metabolites such as NAA, Cr, Cho, Glx, Ins, and GABA.

read frequency spectrum (Puts, 2012). A sample ^1H -MRS spectrum is represented in Figure 2.1, which also displays how different metabolites are chemically separated (Puts, 2012).

For clinical MR imaging chemical shift is generally regarded as an unwanted effect that produces chemical shift artifact between fat and water resonances. However, in ^1H -MRS, this is able to distinguish the hydrogen environments and bonds in respective metabolites (McRobbie, 2006). The spectrum in Figure 2.1 plots signal intensity (approximate metabolite concentration) in the y-axis, and chemical shift on the x-axis (Puts, 2012). Chemical shift is simply metabolite resonant frequency. However, this parameter scales linearly with field, B_0 . Therefore, chemical shift is displayed in field-independent units ppm (parts per million) (Puts, 2012). The ppm metric is a unit that is consistent for each metabolite, independent of magnetic field strength. Therefore the frequency location of a peak remains constant, as it is a quantum property of the hydrogen nuclei

of that specific metabolite (Puts, 2012). Metabolite concentration is a function of y-axis amplitude and changes depending on the tissue of interest (Barantin, 1998). There also lies a challenge, as it is difficult to isolate and identify metabolites of small concentrations such as GABA along the chemical shift axis. Small concentration metabolites can often be overlapped by other more abundant metabolite signals which obscures the small GABA signal (Puts, 2012), as seen in Figure 2.1. Specific ^1H -MRS sequence that target the identification of the metabolite GABA are therefore employed and will be discussed further in this thesis. In order to functionally perform useful ^1H -MRS experiments for the GABA metabolite, it is also necessary to include a localization step to identify where the data is being collected in vivo. Localization of the ^1H -MRS signal is controlled by the operator, where the operator constrains the collection of data to a particular region in the body by exciting signals only within a specific voxel or volume of interest (Stagg, 2011 (2)). Single-voxel ^1H -MRS will be performed in the cervical spinal cord and will additionally be discussed further in this thesis.

Advances in ^1H -MRS methods have shown promising results to identify unique and small concentration metabolites (Henning, 2008; Hock, 2013). This scientific advance has relied upon a strong basis of quantification and reproducibility with regards to ^1H -MRS measurements. Quantification in ^1H -MRS is strongly associated with the selection of a strong reference peak (Barantin, 1998); the ^1H signal of endogenous water has therefore been established as the heteronuclear concentration standard (Barantin, 1998). Tissue concentration of metabolites are further indicated by a ratio to the aforementioned water reference, a method referred to as absolute quantification (Heinzer-Schweizer, 2010). Upon selecting a volume of interest by voxel selection and quantifying a metabolite of interest, the success of the data collection is finally influenced by the signal to noise ratio (SNR) (Puts, 2012). A high SNR is the most important facet of ^1H -MRS data acquisition, as it dictates reliability and reproducibility. SNR, in ^1H -MRS, is proportional to the homogeneity of the magnetic field within a voxel and the voxel volume, and

inversely proportional to the total acquisition time (Puts, 2012). In order to achieve a high quality ^1H -MRS acquisition, a short scan with a very homogenized large voxel is the ideal model. For example, the most often used ^1H -MRS brain acquisition voxel has a $2\times 2\times 2\text{cm}^3$ cubic voxel volume with a 7 minute scan time. However, these specifications are not compatible for other areas of neuronal interest such as the cervical spinal cord (Puts, 2012). This technical limitation will be discussed further in the thesis as placing a ^1H -MRS voxel within the cervical spinal cord is investigated.

Recent technological advancements for ^1H -MRS has generated serious interest for vast fields of neuroscience research. The ability to identify and characterize the location and concentration of precise biochemicals, metabolites, and neurotransmitters offers a more finite and comprehensive view of human brain tissue and its functional processes. ^1H -MRS further offers a valuable insight into the lesser understood human spinal cord, hence making it a unique technology to investigate the neuroplastic behaviour of the human brain through specific concentrations of metabolites such as GABA. The advancement of this technology perpetuates the ability for higher order investigation of the cervical spinal cord and will provide a more thorough understanding of neurological disease.

2.1.2 Cervical Spinal Cord Imaging

Current techniques performed to identify pathological tissue within the spinal cord include a biopsy which is a procedure that is highly invasive and dangerous (Hock, 2013). Therefore, a safer imaging alternative is necessary such as ^1H -MRS. Although quantitative spinal cord ^1H -MRS has mainly been restricted to the brainstem and the upper cervical spine (approximately up to level C3), there exist a variety of challenges in attempting to collect reliable and reproducible data (Henning, 2008). Throughout the many disadvantages of ^1H -MRS, there are a number of researchers providing new methods that can reduce noise, artefacts, and negative effects while boosting signal. Techniques such

as outer volume saturation (OVS), electrocardiographic (ECG) triggering, signal averaging, frequency alignment, and phase corrections can be implemented to improve SNR (Hock, 2013). Apart from reputed SNR boosting techniques, researchers have developed new ways to improve cervical spinal cord acquisition within an MRI setting. For example, work from Stroman (2002) showed that signal enhancement during activation arises predominantly from proton density changes in the extravascular spaces (SEEP), which was applied in spinal cord functional MRI (Stroman, 2002). Saritas (2011), using a diffusion weighted imaging (DWI), demonstrated a relationship between optimal b-values and SNR, therefore improving resulting spinal cord images. In addition, work from De Leener (2016) provided an overview of segmentation methods of the human spinal cord, including application of a Gaussian mean filter that reduces noise and enhances signal quality (De Leener, 2016).

Although some work has impacted the improvement of cervical spinal cord MRI, there remains a significant level of difficulty within ^1H -MRS measurements. Susceptibility differences between non-homogeneous tissues exist in the cervical spine such as between the osseous vertebral bodies, the intervertebral discs, the epidural fat, the transversospino muscle groups, and the vertebral blood vessels (Henning, 2008); a manifestation of the diverse tissue terrain can be seen in Figure 2.2 (Kearney, 2015).

Small cervical spinal cord diameter limits the acquisition voxel size further reducing SNR resulting in poor ^1H -MRS measurements. Often times a rectangular voxel is selected to increase signal in the cervical spinal cord, however this presents difficulties in 'shimming' the voxel adequately (Henning, 2008). Shimming is the ability for the MR system to create a homogenized magnetic field around the specified voxel of interest. Shimming is more precise with smaller cubic geometries and increasingly difficult with long rectangular voxels (Henning, 2008). A typical cervical spine acquisition voxel can also be seen in Figure 2.2 (Kearney, 2015).

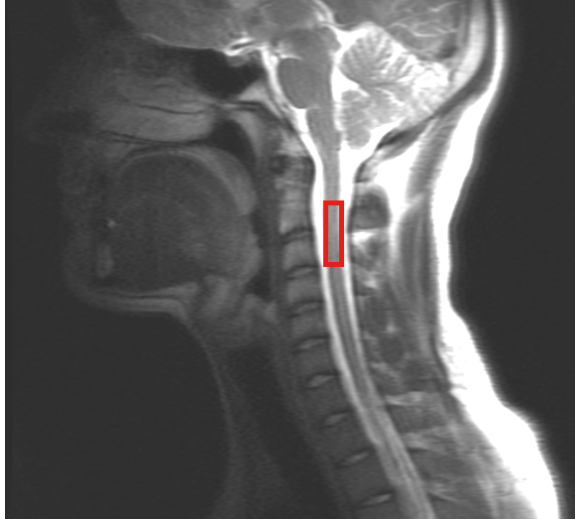


FIGURE 2.2: Voxel selection for a ^1H -MRS cervical spinal cord image is displayed. The inhomogeneity of surrounding tissue and the small voxel is also visible. The above image shows the upper cervical spinal cord of a healthy patient, whereas below, a patient with a cervical spinal cord injury.

The primary technical obstacle in ^1H -MRS is high levels of motion within the cervical spinal cord area. Cardiac and respiratory motion, along with pulsatile flow from vertebral arteries and cerebrospinal fluid (CSF) around the spinal cord induce motion and noise within signal measurements (Henning, 2008). This motion and noise effects the MR parameters B_0 and B_1^+ which highly influence image quality. B_0 and B_1^+ aim to remain constant during measurements, however motion introduces disturbances and variability within these parameters. Therefore, adequate measures must be investigated to reduce motion and increase the stability of B_0 and B_1^+ .

2.1.3 B_0 and B_1^+ Measurements

A key measure to investigate the quality of ^1H -MRS measurements includes the MR parameters B_0 and B_1^+ . Both of these parameters indicate the stability of the MR system and can provide insight on how noise effects signal quality.

The B_0 parameter corresponds to the external magnetic field of an MR system. To understand how this magnetic field influences measurements of biological human tissue, consider the following. Individual protons, or spins, are randomly oriented within the human body, however, when placed within a strong external magnetic field, B_0 , a fraction of spins orient in the same direction as B_0 . A classical physics description dictates that the spins precess at a frequency, known as the Larmor frequency, proportional to the magnitude of the magnetic field B_0 (de Graaf, 1998). This phenomenon can be better understood by Equation 2.1 where γ represents the gyromagnetic ration for protons, equivalent to $2.67 \times 10^8 \text{rad}/(\text{s}\cdot\text{T})$, and ω_0 represents the Larmor frequency :

$$\omega_0 = \gamma B_0 \quad (2.1)$$

In an ideal world, B_0 remains constant, however field variations are often reported due to tissue inhomogeneities, susceptibility, chest motion, and pulsatility effects due to cardiac and respiratory pulses (Martin, 2016; Sclocco, 2017; Van Gelderen, 2007). Therefore, it is necessary to investigate how variability presents itself within the B_0 parameter. Field maps can be acquired to identify the variability of certain areas of anatomy with respect to B_0 . B_0 maps are calculated from phase images (ϕ) acquired at two different scanner echo times (TE) (i.e. the time between the centre of an applied RF pulse and the centre of the resultant MR echo) (Equation 2.2). Mathematically calculating the difference between phases upon the acquisition of two TE's provides a map that represents the variation in B_0 across an area of interest. The B_0 field map units are in frequency (Hz) due to phase changes over time between two TE times.

$$\Delta f = \frac{\phi(TE_2)\phi^*(TE_1)}{2\pi(TE_2 - TE_1)} \quad (2.2)$$

The area of interest studied is often represented by a single slice within a piece of anatomy; in the context of this thesis, a slice was selected in an axial plane within the cervical spinal level of C4. A characteristic B_0 map of the spinal cord at C4 is shown in Figure 2.3.

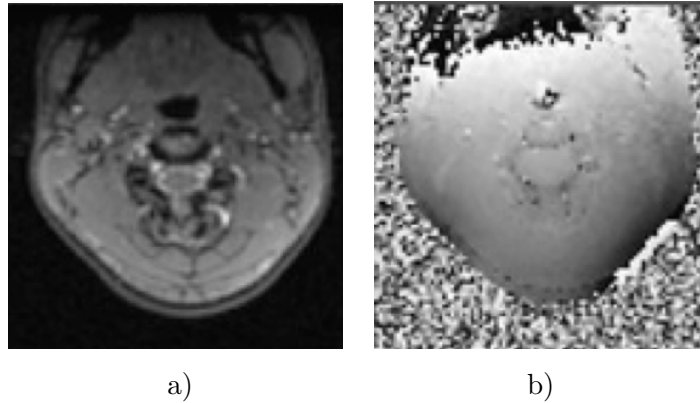


FIGURE 2.3: a) Typical anatomical scan of a healthy human acquired in the axial plane at the spinal level C4. b) Typical B_0 field map of the same healthy human in a), acquired in the same axial plane at the spinal level C4 as in a).

The B_1^+ parameter corresponds to the transmit RF field which perturbs the hydrogen spins, adding energy to them. Vectorially this can be described as spins at equilibrium pointing along Z (i.e. parallel to B_0) being 'torqued' towards the transverse (XY) plane as a result of transmitted RF field. This transmit magnetic field B_1^+ is therefore used to excite hydrogen spins towards an orthogonal plane. The return to equilibrium by the spins releases energy which induces a voltage in a receive RF coil array (i.e. called the B_1^- field). It is also important to mention that the B_1^+ field is proportional to the RF flip angle (α), and this characteristic describes the degree of rotation into the orthogonal field. Changing α is done by changing the strength of the B_1^+ field, as described in Equation 2.3.

$$\alpha = \int_0^T \gamma B_1(t) dt \quad (2.3)$$

In an ideal world, B_1^+ remains constant, however field variations are often reported due to calibration errors in coils, motion, and tissue inhomogeneities between subjects (Ropele, 2005). Therefore, it is additionally necessary to investigate how variability presents itself within the B_1^+ parameter. B_1^+ field maps are acquired in a different fashion compared to B_0 maps. The B_1^+ field maps use the Bloch-Siegert shift mapping method. As there are a variety of sequences that can acquire B_1^+ maps, the Bloch-Siegert method has important advantages such as acquisition speed, accuracy, and robustness (Sacolick, 2010). In the Bloch-Siegert method, a RF pulse of frequency ω_{RF} is applied immediately after excitation. The frequency shift of spins during the off-resonant RF pulse results in a phase shift in the image that can be used to determine the B_1^+ magnitude. The phase shift is acquired using Equation 2.4 (Sacolick, 2010) :

$$\phi_{BS} = \int_0^T \omega_{BS}(t) dt = \int_0^T \frac{(\gamma B_1(t))^2}{2\omega_{RF}(t)} dt \quad (2.4)$$

This equation demonstrates that an expected phase shift can be calculated for any arbitrary pulse $B_1(t)$ with a frequency offset of $\omega_{RF}(t)$. As the B_1^+ parameter is the difference between two phase shifts, two scans must be collected. Therefore, an acquisition with an off-resonance frequency of $+\omega_{RF}$ and another scan with an off-resonance frequency of $-\omega_{RF}$ enables the calculation of B_1^+ . The difference between the two phase shifts provides a variation in B_1^+ across an area of interest. The B_1^+ field map units are in $0.1^\circ/\text{flip angle}$ due to the phase change between the two off-resonance frequency scans. The area of interest studies are often represented by a single slice within a piece of anatomy; in the context of this thesis, a slice is selected in the axial plane within the cervical spinal level of C4. A characteristic B_1^+ field map of the spinal cord at C4 can be seen in Figure 2.4

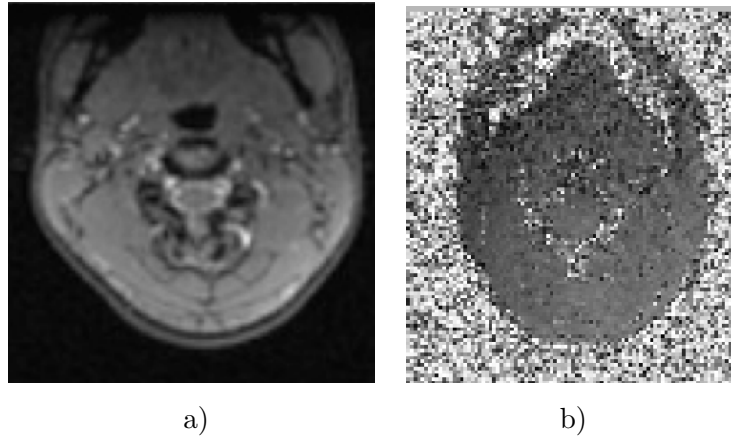


FIGURE 2.4: a) Typical anatomical scan of a healthy human acquired in the axial plane at the spinal level C4. b) Typical B_1^+ field map of the same healthy human in a), acquired in the same axial plane at the spinal level C4 as in a).

2.2 Gamma-Aminobutyric Acid (GABA)

GABA, or Gamma-aminobutyric acid ($H_3N^+CH_2CH_2CH_2COO^-$), is an important neurotransmitter that mainly acts as an inhibitor in the neuronal pathway (Levy, 2013). It is produced from glutamic acid by glutamic acid decarboxylase (GAD) and further broken down by GABA transaminase (GABA-T) (Puts, 2012). GABA is a unique neurotransmitter that is found in two major pools within neurons, cytoplasmic and vesicular, and is only present in lower concentrations ~ 1 mmol/L in human neuronal tissue (Levy, 2013; Puts, 2012; Stagg, 2011 (2)). Cytoplasmic GABA is found throughout GABAergic interneurons and extracellular fluid and is known to play a metabolic role, whereas vesicular GABA is found within the presynaptic boutons and is known to play an inhibitory role for synaptic neurotransmission (Stagg, 2011 (1); Stagg, 2011 (2)). Additionally, there are two major subtypes of GABA receptors: $GABA_A$, which has an inhibitory effect in GABAergic interneurons, and $GABA_B$ which inhibits excitatory potentials and enables long-term potentiation in cortical regions (Levy, 2013, Stagg, 2011 (2)). Due to GABA's inherent ability to induce changes in neuronal function, metabolism, and

recovery, it is investigated in a variety of research areas. Recent efforts have studied inter-individual differences in behavioral performance, early stages of motor learning, and various neurological disorders (Stagg, 2011 (2)). Studying the specific concentrations of GABA on an individual case-by-case basis facilitates a personalized medical approach and is important in evaluating the effect of therapies and treatments for conditions such as epilepsy, motor disorders, mood and anxiety disorders, schizophrenia, alcoholism, drug addiction, sleep disorders, autism spectrum disorders, and olfactory and gustatory disorders (Levy, 2013). GABA agonists are therefore evaluated and observed with regards to their effect in antidepressants and antiepileptic drugs (Levy, 2013). In addition, GABA reduction is known to increase excitatory and vascular reactivity which has generated certain studies to identify GABA and its role in synaptic plasticity and synaptogenesis (Levy, 2013).

The earliest demonstration of GABA identified by ^1H -MRS was accomplished in the 1990s by Rothman (Rothman, 1993). Since Rothman, many advances have been implemented to improve the acquisition of GABA using the ^1H -MRS method. However, there remains challenges with regards to determining accurate and meaningful GABA concentrations such as extracting spectral information with overlapping resonant peaks, different types of brain matter, identifying if the metabolite lies extracellularly or intracellularly, and often times data may not reflect actual neurotransmitter flux and simply measures inactivate GABA pools (Stagg, 2011 (1); Stagg, 2011 (2); Levy, 2013). Regardless, the temporal resolution of current data acquisition schemes are sufficient to reliably detect biologically relevant changes in GABA concentrations within the human cortex (Stagg, 2011 (2)). In order to initially collect spectral data, a ^1H -MRS sequence must first be implemented. A Point RESolved Spectroscopy (PRESS) sequence is a traditional, non-specific, ^1H -MRS sequence that extracts concentration estimates of metabolites such as NAA, Cr, and Cho (de Graaf, 1998). However, a MEGA-PRESS sequence implements a PRESS sequence along with a MESHcher-GARwood (MEGA) method. This provides

additional water suppression and spectral editing due to changing RF amplitudes in order to target specific metabolite such as GABA (Mullins, 2014; de Graaf, 1998).

Although, metabolites such as GABA are most often overlapped by more intense signals such as NAA, a frequency selective RF pulse can be added to the ^1H -MRS sequence to generate another spectrum where only hydrogens resonating near the selected pulse are affected (Puts, 2012; Levy, 2013). Often times a metabolite of interest will possess more than one hydrogen molecule, therefore the appearance of multiplets, or multiple peaks, occurs (Puts, 2012). Multiplets are described as signals influenced by other proximal hydrogens on the same molecule and are further characterized as J-coupling or spin-spin coupling, (seen using the coloured bars in Figure 2.5) (Puts, 2012).

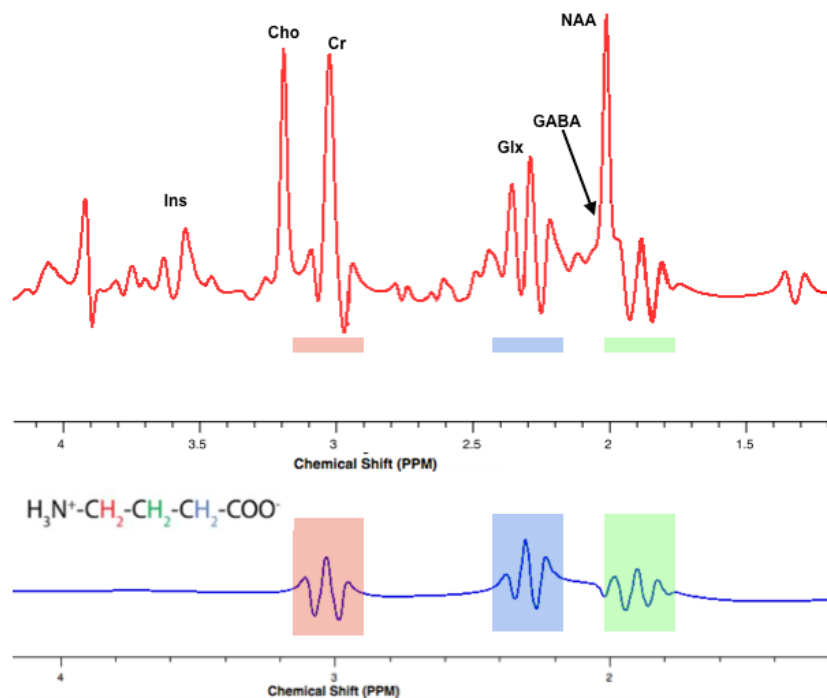


FIGURE 2.5: Typical ^1H -MRS spectrum of the human brain acquired at 3T, showing peaks of neuronal metabolites (i.e. NAA, Cr, GABA). Coloured bars correspond to the peak locations of (b) which represents the GABA ^1H -MRS spectrum. Each colour represents a paired hydrogen and specific chemical signature due to the surrounding molecular environment of hydrogen nuclei within the GABA metabolite.

J-coupling is also a crucial phenomena to identify small concentration metabolites such as GABA due to its unique resonance structure with coupled peaks (Puts, 2012). Spectral editing sequences such as MEGA-PRESS are used to differentiate metabolite peaks based on J-difference-edited approaches (Puts, 2012; Levy, 2013).

There are also other ways to reduce signal overlap such as two-dimensional ^1H -MRS and simply by using higher field MRI scanners. However, for the purpose of this research, spectral editing via MEGA-PRESS was the only approach considered. For MEGA-PRESS, the GABA signal at 3.0 ppm (seen in red in Figure 2.5 (b)) is coupled to the signal at 1.9 ppm (seen in green in Figure 2.5 (b)). If a selective radio-frequency pulse is applied at 1.9 ppm, known as the editing pulse, only metabolites coupled to the 1.9ppm resonance will be affected (i.e. directly affecting the 3.0 ppm coupled resonant peak of GABA) (Puts, 2013, Mullins, 2014). The difference of the pulse centered at 1.9ppm (with GABA resonant coupled peaks) and the original pulse centered at water (including all metabolite peaks) will give a spectrum that only contains signals coupled to the GABA resonant peaks. An example of the MEGA-PRESS process using spectral examples is displayed in Figure 2.6 (Puts, 2012; Mullins, 2014).

There are however certain disadvantages associated with the MEGA-PRESS sequence, including the discrepancy that exists with collecting two different spectra which causes subtraction artifacts and longer scan times, further introducing noise (Puts, 2012). Regardless, the MEGA-PRESS sequence is a tool that allows for proper detection of GABA concentration in-vivo.

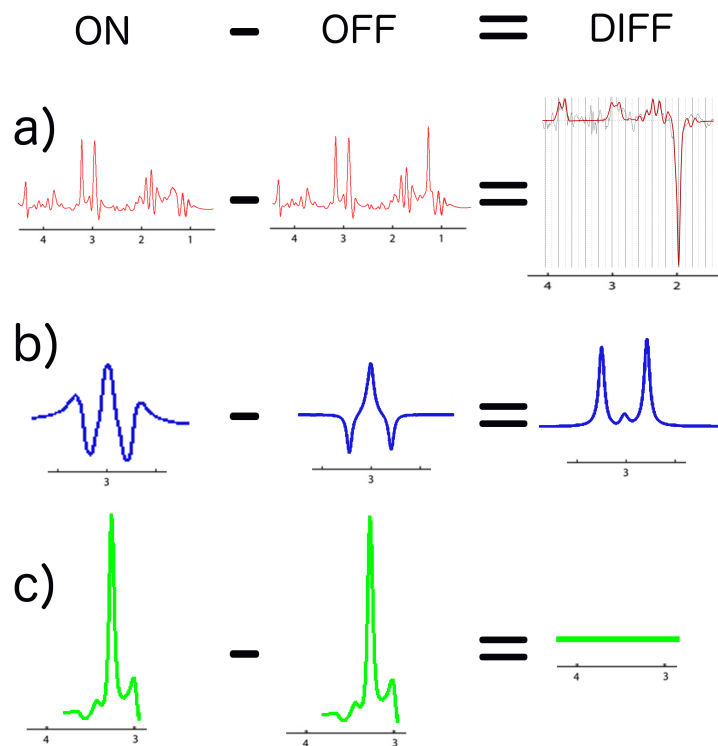


FIGURE 2.6: The complete mechanism of the MEGA-PRESS difference method. In a), the ON editing pulse, left, displays GABA coupled peaks from the selective 1.9 ppm pulse, whereas on the right, in the OFF editing, water is the centered pulse. In b), the difference method is displayed as the 3 ppm GABA signal is clearly shown in the final DIFF spectrum. In c) the difference method demonstrates how subtracting unwanted metabolites occurs as the Choline compounds peak is eliminated from the final DIFF spectrum.

Chapter 3

¹H-Magnetic Resonance

Spectroscopy Phantom Study

3.1 Rationale

Gamma-aminobutyric acid (GABA) is the most prevalent brain inhibitory neurotransmitter and plays a significant role in neuroplasticity. Additionally, it is a crucial component within the cervical spinal cord as its concentrations can reveal information on the upper limb. However, due to low concentrations and chemical spectral peak overlap, GABA is challenging to measure with in vivo ¹H-MRS. Technical nuances create a lack of reproducibility and reliability of cervical spinal cord ¹H-MRS measurements. The primary issue associated with inaccurate measurements remains a lack of signal volume due to restrictions and limitations in voxel size and geometry. In MRS the SNR must be as high as possible, which can only be achieved with either prolonged scan time (SNR $\propto \sqrt{\text{scantime}}$ or large acquisition voxels (SNR \propto voxel volume). Due to the size of the spinal cord, small acquisition voxels placed within the cord greatly reduce SNR, as there is a limited amount of signal volume data collected in the region of interest. As a cubic voxel is implemented as the preferred geometry, to accommodate for lack of signal, a

rectangular voxel can be selected to increase signal volume. This, however, elicits a trade-off with the shimming property of the MR system (Henning, 2008). Shimming is the ability for the MRI to create a spherical homogenized field around a specified voxel (Henning, 2008). It would be too difficult to shim a square object, hence a spherical volume, with the acquired voxel square shape enclosed, is what is preferentially done. Shimming an asymmetric shape such as a rectangular column is more of a challenge for the shimming algorithm used by the MRI system. Therefore investigation of this trade-off relationship must be performed in order to identify the optimal voxel geometry. The aim of Experiment 1 was to assess voxel geometry selection and ensure that reliable data acquisition of an already challenging metabolite, GABA, can be done within a cervical spinal cord shape. This was accomplished through the design and manufacture of a controlled environment (i.e. a GABA spinal cord phantom).

3.2 Hypotheses

A home designed and built phantom was constructed to simulate the cervical spinal cord contents, geometry, and environment. Voxel sizes were manipulated to determine optimal voxel size and geometry, and to determine repeatability and reliability of measurements using a MEGA-PRESS sequence. Metabolite concentrations determined with MRS were compared to known concentrations inside the phantom.

3.3 Methods

3.3.1 Phantom Device

To model and simulate the geometry and contents of the cervical spinal cord, a phantom was constructed. A phantom is a device that is designed with the goal to create a

controlled environment for an imaging setting and is most often a tool used for calibration and quality control. In this experiment, a phantom was constructed to model the cervical spinal cord geometry and test whether GABA could be reliably and repeatably measured. Typically, GABA measurements are performed in the brain, thus this feasibility study is novel due to cord geometry and location.

A phantom was constructed using a cylindrical case composed of acrylic and Poly(methyl methacrylate) with dimensions of 15cm in diameter and 17cm in length. The phantom contained 7 acrylic tubes arranged in a circular arrangement (1cm apart) in the center of the phantom. Dimensions of the 7 acrylic tubes were specifically ordered to match the average size of an adult human cervical spinal cord (9mm anterior-posterior, 12mm axially) (Sherman, 1990). The 7 acrylic tubes were filled with one of three solutions (BRAINO (General Electric Healthcare, Milwaukee, WI, USA), BRAINO + 10mM GABA, and 5mM GABA) (Lattanzi, 2010). BRAINO solution is a QA/QC standard used by General Electric Healthcare as a 'brain' tissue phantom and its specific contents can be seen in Figure 3.1 below.

Concentration	Symbol	Chemical
50 mM	KH ₂ PO ₄	potassium phosphate monobasic
56 mM	NaOH	sodium hydroxide
12.5 mM	NAA	N-acetyl-L-aspartic acid
10.0 mM	Cr	creatine monohydrate
3.0 mM	Ch	choline chloride
7.5 mM	ml	Myo-inositol
12.5 mM	Glu	L-glutamic acid (monosodium salt)
5.0 mM	Lac	DL-lactic acid (lithium salt)
0.10%	Azide	sodium azide
0.10%	GdDPTA	Magnavest

FIGURE 3.1: The entire contents of BRAINO solution including the concentrations of specific metabolites. Some chemicals are included to preserve the phantom over time, whereas key metabolites NAA, Cr, Cho, ml, Glu, and Lac are included to mimic neuronal tissue contents.

BRAINO contains the same biochemical metabolites along with similar concentrations to those found within typical healthy brain tissue. The phantom was then filled with 3% agarose gel (containing 0.1% sodium azide (NaN_3) preservative) (Lattanzi, 2010) to lower magnetic susceptibility differences that would be present between acrylic and air (Hellerbach, 2013). The phantom can be seen in Figure 3.2 a) whereas a localizing MRI scan of the phantom can be seen in Figure 3.2 b). Imaging was performed using a GE MR750 3T MRI (General Electric Healthcare, Milwaukee, WI) and a MR Instruments 32-channel head coil.

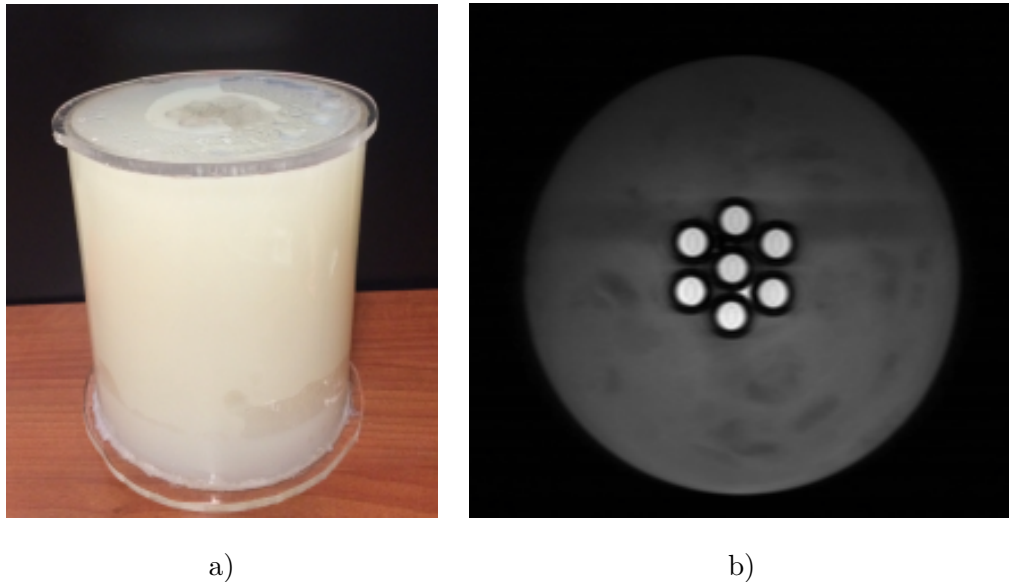


FIGURE 3.2: A constructed cervical spinal cord phantom. a) represents a three-dimensional view of the phantom post-production. b) represents an MR scan of the phantom where the 7 acrylic tubes in the center filled with solution (white) are easily identifiable along with the surrounding agarose gel (grey).

3.3.2 ^1H -MRS Sequences and Protocols

^1H -MRS acquisitions were performed using both PRESS (TE/TR = 35/1500 ms, NEX = 256) and MEGA-PRESS (TE/TR = 68/1500 ms, NEX = 256) sequences. MEGA-PRESS was utilized to investigate the concentration of the GABA + BRAINO and

GABA only solutions to therefore identify the GABA peaks within these volumes. The PRESS sequence was utilized as a quality assurance tool to identify that BRAINO and GABA + BRAINO solutions were reliably measuring all metabolites within these volumes. Each tube was investigated with both sequences with identical voxel placements for each tube. Voxel dimensions of $1 \times 1 \times 1 \text{cm}^3$ (1cm^3), $1 \times 1 \times 2 \text{cm}^3$ (2cm^3), and $1 \times 1 \times 3 \text{cm}^3$ (3cm^3) were placed in the center of each tube and further evaluated. Due to cylindrical geometries of interest, voxel shimming was crucial for success of this study as full width half maximum (FWHM) linewidths above 4Hz were rejected (Drost, 2002). The phantom was stored in the MR scanner room where temperatures ranged from 19.2°C to 21.3°C . Therefore the scanner control variable *tempC* was hardcoded each scanning session to ensure minimal temperature variability. Spectra were analyzed using the LCModel software package (Provencher, 1993).

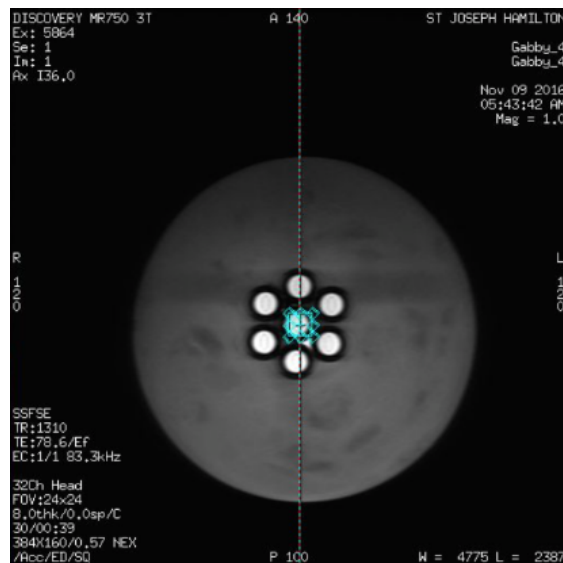


FIGURE 3.3: The voxel positioning used in the phantom to evaluate Experiment 1. The voxel was placed within the center of each acrylic tube and acquired data was analyzed and compared to known concentrations

3.3.3 Analysis Pipeline

For phantom repeatability assessment, 7 scanning sessions were performed on the phantom. The scanning included the implementation of both the PRESS and MEGA-PRESS sequences on the BRAINO, BRAINO + GABA, and GABA solution tubes. . The GABA + BRAINO solution contains 10mM of GABA metabolite, and the GABA-only solution contain 5mM of GABA metabolite. For each PRESS scan, the metabolites Cho, Cr, GABA, Glu (Glutamic acid), Lac, (Lactate), ml (myo-Inositol) and NAA were investigated to ensure accuracy for each solution type with respect to the known BRAINO concentrations. For each MEGA-PRESS scan, only GABA and NAA metabolites were investigated. Additionally, for each scan, the voxel size was evaluated at $1 \times 1 \times 1 \text{cm}^3$, $1 \times 1 \times 2 \text{cm}^3$, and $1 \times 1 \times 3 \text{cm}^3$, respectively, where the change in dimension corresponds to the z-direction (i.e. along the length of the mock spinal cord in the phantom). The acquisition voxel position is shown in Figure 3.3. PRESS spectra were analyzed with the LCModel software package using the following parameters :

Analyzing spectrum from	4.2ppm down to 0.2 ppm
Select	Do eddy-current correction
Select	Do water-scaling
Select Basis files	ge_press_te35_3T_0.1a.basis
Control Defaults file	standard
Execution Script	IRC-standard

MEGA-PRESS spectra were also analyzed using LCModel using the same parameters as above, however with the following spectral basis set:

Select Basis files	3T_GE_MEAGAPRESS_Kaiser.basis
--------------------	-------------------------------

3.4 Results and Discussion

3.4.1 LCModel analysis of the PRESS sequence

Concentration estimates using LCModel for the 7 phantom scanning sessions using a PRESS sequence are shown in Figure 3.4. LCModel was found to provide reliable spectral analysis and concentration estimates of the BRAINO and BRAINO+GABA solutions, specifically within the $1 \times 1 \times 2 \text{cm}^3$ voxel. This was confirmed using a 2-tailed type 3 T-test comparing the actual concentrations with estimates from LCModel. It should be noted that measurements were rejected with significantly poorer shim (here classified as not be able to achieve a full width half-maximum (FWHM) under 4 Hz). No $1 \times 1 \times 3 \text{cm}^3$ voxel satisfied these constraints. Thus, following experiments were carried out with $1 \times 1 \times 1 \text{cm}^3$ and $1 \times 1 \times 2 \text{cm}^3$ voxels only, at a penalty of SNR.

For the GABA-only solution, LCModel fitting continually failed. This was because the basis sets within LCModel attempt to estimate concentrations of metabolites which are in fact not present within the solution, therefore LCModel failed in this regard as it tries to estimate concentrations above 0 for all metabolites (excluding GABA). The estimated concentrations, standard deviations, and the p-values compared to the actual expected concentration for each metabolite can be found in Figure 3.5. A key observation to note was the $1 \times 1 \times 1 \text{cm}^3$ voxels provided significantly poor results compared to $1 \times 1 \times 2 \text{cm}^3$ voxels. The increase in reliability can be inferred as a larger volume of investigation increases signal which increases SNR. Also, most metabolites provide reliable measurements within the $1 \times 1 \times 2 \text{cm}^3$ voxel including Cr, Cho, mI, Glu, Lac, and GABA as their p-values adhere to under 0.05. Finally, GABA at 5mM of concentration within the GABA-only solution was measured appropriately and repeatably in the $1 \times 1 \times 2 \text{cm}^3$ voxel.

Analysis of BRAINO-only solutions reflected more accurate measurements than GABA-only solutions. Although most metabolites were appropriately estimated within each

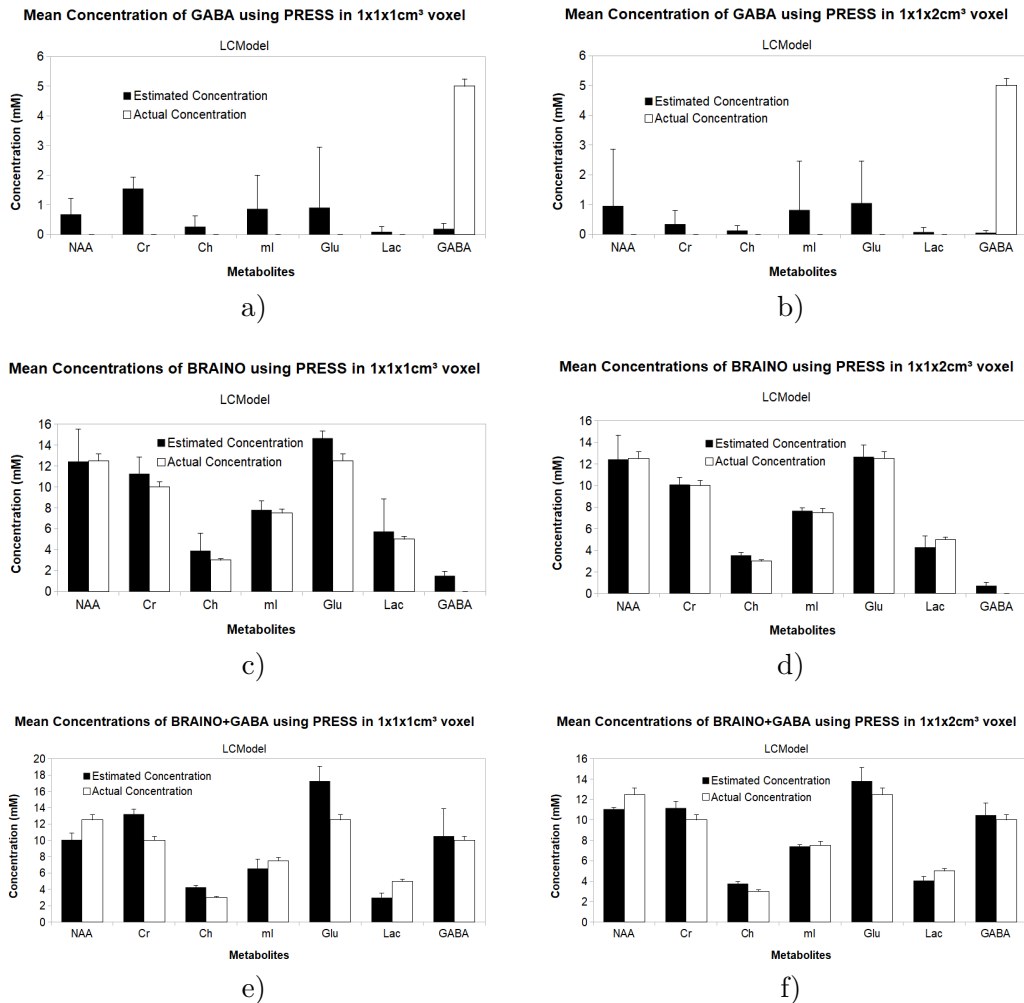


FIGURE 3.4: Graphical representation of the mean concentrations of metabolites found in GABA, BRAINO, or BRAINO+GABA solutions using the PRESS sequence in a selected voxel size (i.e. $1 \times 1 \times 1 \text{cm}^3$ or $1 \times 1 \times 2 \text{cm}^3$). The mean ($n=7$) estimated concentrations by LCMModel of metabolites (NAA, Cr, Ch, ml, Glu, Lac, and GABA) are shown in black, whereas the actual concentrations are shown in white. Positive standard deviations are also represented by black error bars. Figures a), c), and e) show concentrations within a selected $1 \times 1 \times 1 \text{cm}^3$ voxel for GABA, BRAINO, and BRAINO+GABA solutions respectively. Figures b), d), and f) show concentrations within a selected $1 \times 1 \times 2 \text{cm}^3$ voxel for GABA, BRAINO, and BRAINO+GABA solutions respectively.

	Actual Concentration (mM)	Actual Standard Deviation (%)	1x1x1cm ³ Voxel Concentration (mM)	1x1x1cm ³ Standard Deviation (%)	1x1x1cm ³ P-Value (T-test)	1x1x2cm ³ Voxel Concentration (mM)	1x1x2cm ³ Standard Deviation (%)	1x1x2cm ³ P-Value (T-test)
NAA	0	0	0.6838	0.5432	0.0195	0.9563	1.9012	0.1745
Cr	0	0	1.5512	0.3825	0.0000	0.3472	0.4595	0.0259
Cho	0	0	0.2700	0.3530	0.0268	0.1293	0.1651	0.0227
ml	0	0	0.8668	1.1311	0.0784	0.8198	1.6395	0.0862
Glu	0	0	0.9116	2.0384	0.0862	1.0530	1.4144	0.0274
Lac	0	0	0.0942	0.1815	0.1201	0.0759	0.1494	0.0832
GABA	5	0.2500	0.1959	0.1757	0.0068	0.0573	0.0580	0.0081

a) GABA Solution

	Actual Concentration (mM)	Actual Standard Deviation (%)	1x1x1cm ³ Voxel Concentration (mM)	1x1x1cm ³ Standard Deviation (%)	1x1x1cm ³ P-Value (T-test)	1x1x2cm ³ Voxel Concentration (mM)	1x1x2cm ³ Standard Deviation (%)	1x1x2cm ³ P-Value (T-test)
NAA	12.5	0.6250	12.435	3.0833	0.2804	12.442	2.2107	0.3624
Cr	10	0.5000	11.270	1.5829	0.0248	10.108	0.6544	0.0176
Cho	3	0.1500	3.9158	1.6786	0.0000	3.5453	0.2403	0.0004
ml	7.5	0.3750	7.7998	0.8658	0.1635	7.6735	0.2848	0.0980
Glu	13	0.6250	14.667	0.6536	0.0001	12.675	1.0630	0.0455
Lac	5	0.2500	5.7414	3.1026	0.3334	4.2933	1.0561	0.0814
GABA	0	0	1.5122	0.3891	0.0504	0.7424	0.2906	0.0004

b) BRAINO Solution

	Actual Concentration (mM)	Actual Standard Deviation (%)	1x1x1cm ³ Voxel Concentration (mM)	1x1x1cm ³ Standard Deviation (%)	1x1x1cm ³ P-Value (T-test)	1x1x2cm ³ Voxel Concentration (mM)	1x1x2cm ³ Standard Deviation (%)	1x1x2cm ³ P-Value (T-test)
NAA	12.5	0.6250	10.069	0.7962	0.0135	11.072	0.1307	0.0000
Cr	10	0.5000	13.226	0.6261	0.0036	11.177	0.6583	0.0021
Cho	3	0.1500	4.2734	0.2465	0.0182	3.7678	0.2165	0.0001
ml	7.5	0.3750	6.571	1.1440	0.0554	7.4098	0.1803	0.0379
Glu	13	0.6250	17.273	1.7729	0.0002	13.821	1.3243	0.0494
Lac	5	0.2500	2.9834	0.5735	0.0000	4.0706	0.3824	0.0001
GABA	10	0.5000	10.538	3.3581	0.3719	10.474	1.1676	0.1807

c) BRAINO+GABA Solution

FIGURE 3.5: The 2 tailed type 3 T-test results for the GABA, BRAINO, and BRAINO+GABA solutions using the PRESS sequence are represented here. The actual and estimated concentrations by LCMoDel along with respective standard deviations are shown. The P-value result of the T-test comparing estimated vs. actual concentrations for each metabolite are also shown. Measurements were conducted within 1x1x1cm³ (left-most columns) and 1x1x2cm³ voxels (right-most columns). Figures a), b), and c) show all of the statistical values in GABA, BRAINO, and BRAINO+GABA solutions respectively.

voxel, the estimated concentration of GABA, which was not present within the solution, was not accurately measured. As seen in Figure 3.4 and Figure 3.5, some key conclusions regarding this data can be identified. Mainly, as seen in the GABA-only solution, the $1 \times 1 \times 2 \text{ cm}^3$ voxel ($n=7$) provided more reliable measurements than the $1 \times 1 \times 1 \text{ cm}^3$ voxel ($n=7$). Also, most metabolites, including GABA provided very reliable measurements within the $1 \times 1 \times 2 \text{ cm}^3$ voxel including Cr, Cho, mI, Glu, Lac, and GABA as their standard deviations were all under 1.1% and their p-values adhere to under 0.05 within the context of a 2-tailed type 3 T-test.

Analysis of the BRAINO+GABA solutions reflected accurate measurements for NAA, Cr, Cho, mI, Glu, and Lac metabolites, however, not for GABA. Although most metabolites were appropriately estimated, the estimated concentration of GABA, which was 10mM, was estimated accurately within the context of its mean. However, this was not a precise measurement as its 2-tailed T-test generated a p-value of 0.18. As seen in Figure 3.4 and Figure 3.5 shows the $1 \times 1 \times 2 \text{ cm}^3$ voxel ($n=7$) provided more reliable measurements than the $1 \times 1 \times 1 \text{ cm}^3$ voxel ($n=7$). Also, the NAA metabolite was repeatably and reliably measured along with Cr, Cho, mI, Glu, and Lac within the $1 \times 1 \times 2 \text{ cm}^3$ voxel. Finally, NAA, Cr, Cho, mI, Glu, and Lac metabolites were all estimated using LCModel within the $1 \times 1 \times 1 \text{ cm}^3$ voxel.

3.4.2 LCModel analysis of the MEGA-PRESS sequence

The second analysis step involved estimating metabolite concentrations for the 7 phantom scanning sessions using a MEGA-PRESS sequence. Again, as above, the LCModel software package was used for analysis Figure 3.6. It provided very reliable spectral analysis and concentration estimates of GABA within the GABA, BRAINO, and BRAINO+GABA solutions using MEGA-PRESS sequence, specifically within the $1 \times 1 \times 2 \text{ cm}^3$ voxel. This was confirmed by comparing the actual concentrations (with experimental

error) and the concentration estimates of the LCModel software. Measurements were also rejected from this analysis if data had poor SNR and/or could not be shimmed to have a full width at half maximum (FWHM) of less than 4Hz. As with the PRESS sequence the tests using $1 \times 1 \times 3 \text{cm}^3$ voxels could not satisfy these constraints. The further analysis was then only done on the $1 \times 1 \times 1 \text{cm}^3$ and $1 \times 1 \times 2 \text{cm}^3$ acquisition voxels. Finally, it should be noted that only NAA and GABA concentrations could be estimated as the MEGA-PRESS sequence is designed specifically to only measure GABA, with NAA being a reference metabolite.

For the solution containing only GABA, unlike the PRESS sequence, NAA was repeatably estimated regardless of voxel size. This was quite odd however, as there was no NAA present in the GABA-only solution. However, the GABA metabolite in the same solution was accurately and repeatably estimated within the $1 \times 1 \times 2 \text{cm}^3$ voxel. It seems that LCModel assessment of MEGA-PRESS data is reliable for studies where solutions contain only GABA (e.g. phantom or reference scans), where the voxel size exceeds 2cm^3 . Additional observations regarding the estimated concentrations, the standard deviations, and the p-values compared to the actual expected concentration for NAA and GABA are shown in Figure 3.7. Measurements within the $1 \times 1 \times 1 \text{cm}^3$ voxel (n=7) were significantly poorer at estimating the concentration compared to the $1 \times 1 \times 2 \text{cm}^3$ voxel (n=7). Also, the estimated GABA concentration in the $1 \times 1 \times 2 \text{cm}^3$ voxel, compared to the smaller voxel, was significantly lower ($p < 0.05$; 2-tailed T-test). The LCmodel determined concentration from the larger acquisition voxel was 4.5 ± 0.63 , where the actual concentration was 5mM. From this it was determined that phantom measures were reliable measurement.

Analysis of the BRAINO-only solutions reflected even more accurate measurements than the strong GABA-only solution estimations detailed above. Although NAA was not

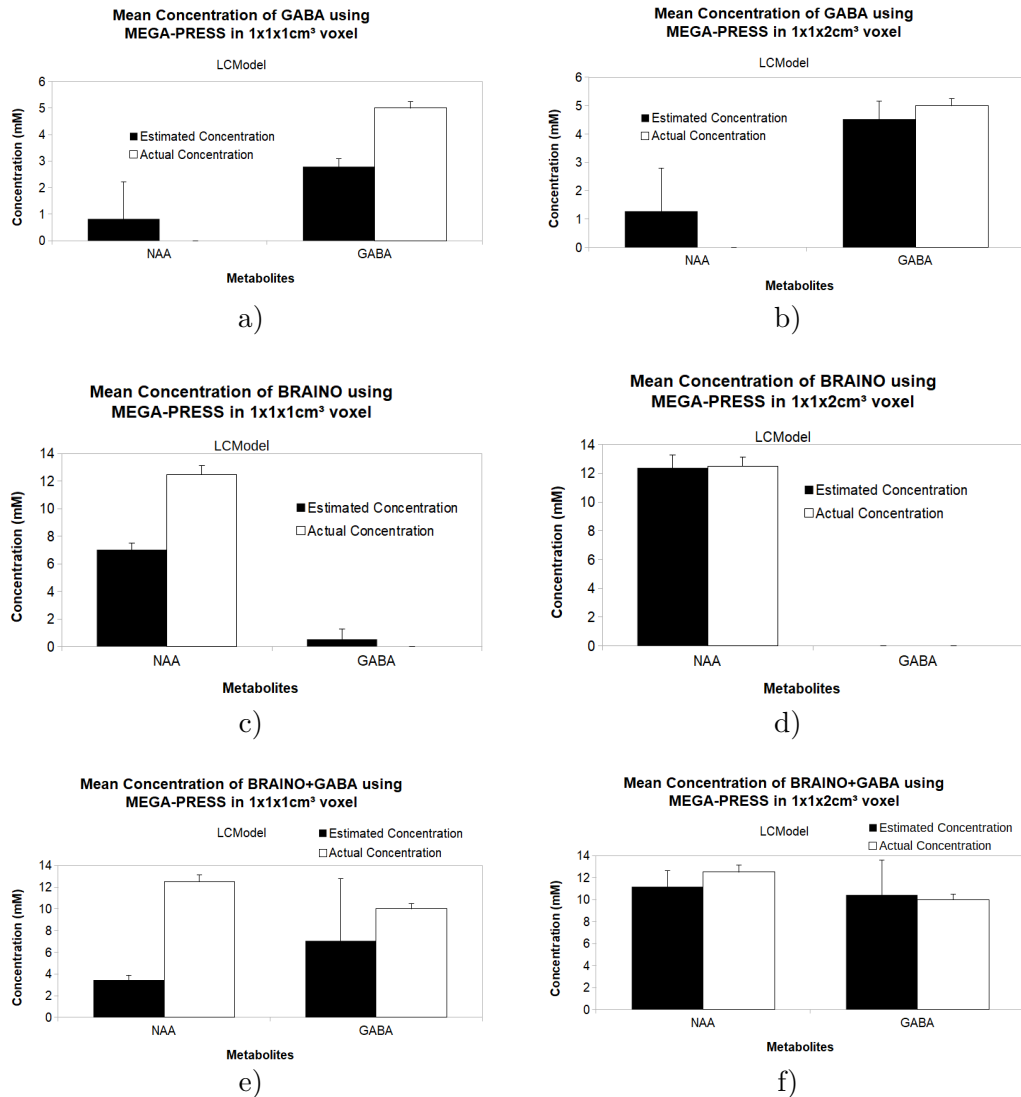


FIGURE 3.6:]

Graphical representation of the mean concentrations of metabolites found in GABA, BRAINO, or BRAINO+GABA solutions using the MEGA-PRESS sequence in a selected voxel size (i.e. 1x1x1cm³ or 1x1x2cm³). The mean (n=7) estimated concentrations by LCMoDel of metabolites (NAA and GABA) are shown in black, whereas the actual concentrations are shown in white. Positive standard deviations are also represented by black error bars. Figures a), c), and e) show concentrations within a selected 1x1x1cm³ voxel for GABA, BRAINO, and BRAINO+GABA solutions respectively. Figures b), d), and f) show concentrations within a selected 1x1x2cm³ voxel for GABA, BRAINO, and BRAINO+GABA solutions respectively.

	Actual Concentration (mM)	Actual Standard Deviation (%)	1x1x1cm ³ Voxel Concentration (mM)	1x1x1cm ³ Standard Deviation (%)	1x1x1cm ³ P-Value (T-test)	1x1x2cm ³ Voxel Concentration (mM)	1x1x2cm ³ Standard Deviation (%)	1x1x2cm ³ P-Value (T-test)
NAA	0	0	0.8187	1.4040	0.0869	1.2767	1.5249	0.0669
GABA	5	0.2500	2.7900	0.3063	0.0625	4.5286	0.6319	0.0490

a) GABA Solution

	Actual Concentration (mM)	Actual Standard Deviation (%)	1x1x1cm ³ Voxel Concentration (mM)	1x1x1cm ³ Standard Deviation (%)	1x1x1cm ³ P-Value (T-test)	1x1x2cm ³ Voxel Concentration (mM)	1x1x2cm ³ Standard Deviation (%)	1x1x2cm ³ P-Value (T-test)
NAA	12.5	0.6250	7.0300	0.4781	0.2394	12.390	0.8773	0.0810
GABA	0	0	0.5222	0.7379	0.0326	0	0	0

b) BRAINO Solution

	Actual Concentration (mM)	Actual Standard Deviation (%)	1x1x1cm ³ Voxel Concentration (mM)	1x1x1cm ³ Standard Deviation (%)	1x1x1cm ³ P-Value (T-test)	1x1x2cm ³ Voxel Concentration (mM)	1x1x2cm ³ Standard Deviation (%)	1x1x2cm ³ P-Value (T-test)
NAA	12.5	0.6250	3.4434	0.4514	0.2904	11.184	1.4290	0.0429
GABA	10	0.5000	7.0600	5.7184	0.2671	10.432	3.1383	0.0269

c) BRAINO+GABA Solution

FIGURE 3.7: The 2 tailed T-test results for the GABA, BRAINO, and BRAINO+GABA solutions using the MEGA-PRESS sequence. The actual and estimated concentrations by LCMoDel along with respective standard deviations are shown. The P-value result of the T-test comparing estimated vs. actual concentrations for each metabolite (NAA and GABA) are also shown. Measurements were conducted within 1x1x1cm³ (left-most columns) and 1x1x2cm³ voxels (right-most columns). Figures a), b), and c) show all of the statistical values in GABA, BRAINO, and BRAINO+GABA solutions respectively.

accurately measured in the 1x1x1cm³ voxel (n=7), GABA in the 1x1x1cm³ voxel (n=7) and both GABA and NAA in the 1x1x2cm³ voxel (n=7) were appropriately estimated (p<0.05; 2-tailed T-test). As in the GABA-only solution, the BRAINO-only solution provided reliable measurements with the absence of GABA and the presence of BRAINO metabolites, specifically within the 1x1x2cm³ voxel.

Analysis of the BRAINO+GABA solutions reflected similar observations as the above BRAINO-only solution, however, only within the 1x1x2cm³ voxel (n=7). The 1x1x1cm³ voxel (n=7) yielded poor and inaccurate results for NAA and GABA as seen in Figure

3.6 and Figure 3.7. The $1 \times 1 \times 2 \text{cm}^3$ voxel yielded near concentration estimates for both GABA and NAA, with standard deviations below 1.5% and p-values below 0.05. The BRAINO+GABA solution estimates using LCMoel provided reliable and repeatable measurements for future GABA investigation.

Undoubtedly measurement reliability is critical before measuring GABA in vivo. To ensure that data was appropriate in terms of MRI scanner consistency (i.e. to verify instrument inconsistency did not affect outcome), a number of scanner parameters were assessed. First, during spectral fitting residual errors ($|\text{observed-expected}|$) were plotted along with the fit. Residuals were considered with regards to quality of data, as a noisy residual error would be characterized by high frequency noise. The spectral fitting identifies which metabolites are present (plus their amounts). A noisy fit prevents the ability to correctly identify metabolites and determine their concentrations. It is important to note that fitting accuracy also changes depending on the metabolites present (i.e. GABA, BRAINO, or BRAINO+GABA) and the sequence employed (i.e. PRESS or MEGA-PRESS). Secondly, Q values for each fit were recorded (mean $Q=1.92 \pm 0.66$) ensuring no dramatic changes in SNR or magnetic field homogeneity occurred. Next, before proceeding with each scan, a spectral 'auto pre-scan' was performed to ensure the voxel size was appropriately shimmed to yield a FWHM below 4Hz. All scans ($n=14$) for each solution ($N=42$ in total) had a FWHM of either 1Hz or 2Hz. Finally, the MRI system transmit and receiver gains were evaluated to determine if their variability could contribute to spectral quality. Receiver gains did not change for any scan ($R1=13$, $R2=30$) and the transmit gain for PRESS ($TG=108.11 \pm 1.00$) and MEGA-PRESS ($TG=94.78 \pm 1.50$) did not differ throughout the study.

Chapter 4

Comparison of ^1H -MRS Software Tools

4.1 Rationale

^1H -MRS data is useful for investigating the biochemical nature of tissues. Often radiologists perform subjective assessment of spectra that are not quantifiable or reproducible. For proper interpretation a sound analysis pipeline is essential. There are a large number of software tools available that are either free to download (from repositories such as Sourceforge) or are proprietary (and hence costly). To estimate metabolite concentrations and to visualize the spectrum, two popular software tools that are available are TARQUIN (freely downloadable) and LCModel (proprietary). These software tools can both analyze raw ^1H -MRS data, and both perform a similar algorithm to the analysis: both employ a linear combination of basis spectra and estimate concentrations of metabolite peaks using the water peak as a reference (Saleh, 2016). LCModel remains the research standard software tool as it is commercially available and uses proprietary knowledge of metabolite basis spectra to fit GABA in the frequency domain (Saleh,

2016). LCModel additionally uses a linear combination of metabolites, lipids, and macromolecules combined with smoothing splines to account for baseline signals (Kossowski, 2017). Although LCModel is a comprehensive and respected tool with an abundance of features and allows for in-depth analysis, the costs are substantial. Therefore, a new software tool in TARQUIN requires consideration. TARQUIN is a freely available software which performs similar measurements, however implements a time-domain fitting combined with an algorithmic approach compared to the frequency domain approach of LCModel (Kossowski, 2017). In addition, TARQUIN utilizes non-negative least squares projections to estimate metabolite amplitudes along with simulated metabolite, lipid, and macro-molecule basis sets (Kossowski, 2017). Although there exists inherent differences between both software packages, the end results may be significantly similar. A comparative investigation and analysis of both of these software packages is therefore warranted to determine if TARQUIN is an appropriate alternative for the costly LCModel.

4.2 Hypotheses

Because both software packages perform similarly, and both are relatively popular, TARQUIN and LCModel were compared. A home built and designed phantom, with known metabolite concentrations, was used in order to standardize measurements between both software packages and allow for a controlled comparison. The hypothesis was that both software packages performed equally as well, with similar reliability and reproducibility.

4.3 Methods

4.3.1 Phantom Device

This software comparison study was performed using the same phantom as detailed in Chapter 3. The phantom establishes a known 'constant' in order to compare both software packages to the same MRS measurement acquisitions. The phantom in this sense was utilized as an objective calibration tool for ^1H -MRS measurements.

4.3.2 ^1H -MRS Sequences and Protocols

^1H -MRS acquisitions were performed using MEGA-PRESS (TE/TR = 68/1500ms, NEX = 256) and PRESS (TE/TR = 35/1500ms, NEX=256) sequences. The same solution volumes were investigated as detailed Chapter 3 (i.e. GABA, BRAINO, BRAINO+GABA). Only voxels of $1\times 1\times 1\text{cm}^3$ and $1\times 1\times 2\text{cm}^3$ were used as the $1\times 1\times 3\text{cm}^3$ acquisition volume was not adequate in terms of shim and SNR (Chapter 3).

4.3.3 Analysis Pipeline

For the analysis, 7 MRS scans were collected from each of the sample tubes in the phantom (i.e. GABA, BRAINO, and BRAINO + GABA). MRS PRESS (n=7) and MEGA-PRESS (n=7) scans were acquired using $1\times 1\times 1\text{cm}^3$ and $1\times 1\times 2\text{cm}^3$ voxels, respectively. The raw data (i.e. time domain data) were saved and used in subsequent analysis. The GE Healthcare MRI platform saves raw data in what called a 'Pfile'. Along with proprietary header information, these files contain an unsuppressed water spectrum and time domain data saved for each complete cycle of the RF phase (i.e. if the phase is cycled 8 times and the scan is 256 averages then there are 256/8 or 64 lines of time domain data stored in the raw format). GE Healthcare is the only MRI vendor to store

MRS data this way- other vendors require the user to also acquire a non-water suppressed MR spectrum for water scaling. Raw data files are easily read by both TARQUIN and LCModel.

For TARQUIN, the Pfile is selected as both the data file and water suppressed data file. For the PRESS sequence the following parameters were implemented:

Pulse Sequence	PRESS
Dynamic freq. correction	(check this box)
Dynamic correlation reference signals (WS)	1H Cr Cho
Reference Offset (ppm)	4.85
Reference Signals	1H NAA
Start Point	5
Water Concentration	55556
Internal Basis Set	1H BRAINO phantom

For MEGA-PRESS scans in TARQUIN, the Pfile was selected as the water suppressed data file (same as above) and the same parameters were implemented (as above) with the following differences:

Pulse Sequence	MEGA-PRESS
Internal Basis Set	1H MEGA-PRESS GABA

Comparative analysis focused on concentration estimates of metabolites and their residual values, standard deviation and p-values (i.e. whether the metabolite was adequately fitted by the algorithm). Subsequently, a T-test between both software packages

was used to identify whether software packages provided equal information.

4.4 Results and Discussion

4.4.1 TARQUIN analysis of the PRESS sequence

Similar to the analysis performed in the previous chapter (Chapter 3), concentration estimates were identified for the 7 phantom scanning sessions using data collected using a PRESS sequence. TARQUIN analysis results are shown in Figure 4.1. The TARQUIN package provided reliable spectral analysis and concentration estimates of the BRAINO and BRAINO+GABA solutions only for the $1 \times 1 \times 2 \text{cm}^3$ voxel. This was confirmed by comparing the spectral fitted values to actual concentrations (with experimental error). As in previous experiments, measurements were rejected if they had significant noise and could not be shimmed to a FWHM $< 4\text{Hz}$.

Analysis of the GABA-only solution provided similar results to LCModel where the $1 \times 1 \times 1 \text{cm}^3$ acquisition voxel ($n=7$), no metabolites were properly estimated including GABA. TARQUIN therefore similarly failed in this regard as it estimated concentrations above 0 for all metabolites when none of NAA, Cr, Ch, mI, Glu, Lac were present. Additional observations regarding the estimated concentrations, the standard deviations, and the p-values compared to the actual expected concentration for each metabolite are shown in Table 4.2. Although metabolite concentrations were repeatable within the $1 \times 1 \times 2 \text{cm}^3$ voxel ($n=7$), they were incorrect in their concentration estimates. The only acceptable measure to extrapolate from the TARQUIN analysis in the GABA-only solution, was the measure of GABA in the $1 \times 1 \times 2 \text{cm}^3$ voxel, where its p-value was below 0.05, with a standard deviation of 4.6%. In these samples TARQUIN performed similarly to LCModel.

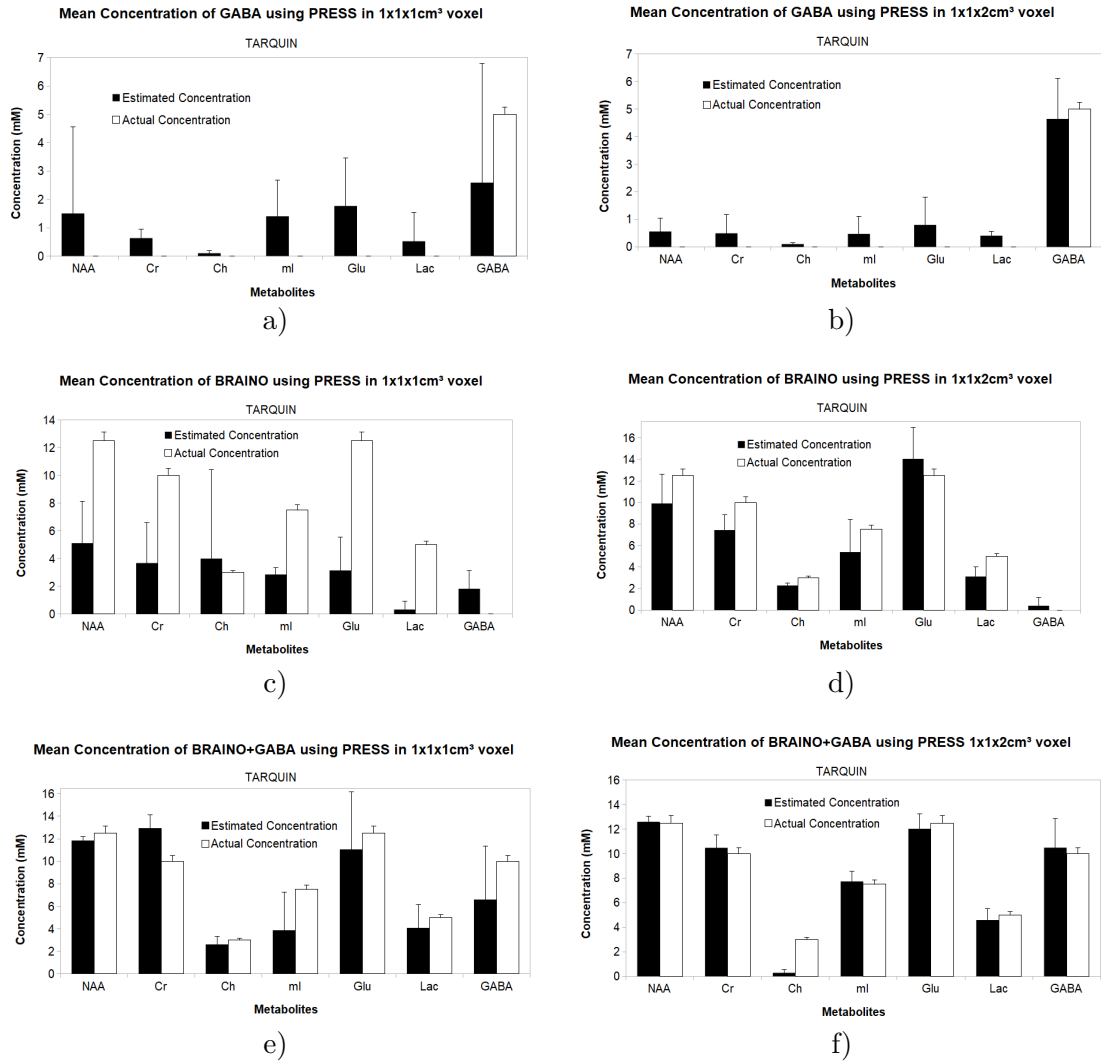


FIGURE 4.1: Graphical representation of the mean concentrations of metabolites found in GABA, BRAINO, or BRAINO+GABA solutions using the PRESS sequence in a selected voxel size (i.e. $1 \times 1 \times 1 \text{cm}^3$ or $1 \times 1 \times 2 \text{cm}^3$). The mean ($n=7$) estimated concentrations by TARQUIN of metabolites (NAA, Cr, Ch, ml, Glu, Lac, and GABA) are shown in black, whereas the actual concentrations are shown in white. Positive standard deviations are also represented by black error bars. Figures a), c), and e) show concentrations within a selected $1 \times 1 \times 1 \text{cm}^3$ voxel for GABA, BRAINO, and BRAINO+GABA solutions respectively. Figures b), d), and f) show concentrations within a selected $1 \times 1 \times 2 \text{cm}^3$ voxel for GABA, BRAINO, and BRAINO+GABA solutions respectively.

	Actual Concentration (mM)	Actual Standard Deviation (%)	1x1x1cm ³ Voxel Concentration (mM)	1x1x1cm ³ Standard Deviation (%)	1x1x1cm ³ P-Value (T-test)	1x1x2cm ³ Voxel Concentration (mM)	1x1x2cm ³ Standard Deviation (%)	1x1x2cm ³ P-Value (T-test)
NAA	0	0	1.5053	3.0628	0.0677	0.5594	0.5594	0.0107
Cr	0	0	0.6328	0.3210	0.0023	0.4935	0.4935	0.0289
Cho	0	0	0.1039	0.0852	0.0237	0.0983	0.0983	0.0009
ml	0	0	1.4051	1.2744	0.0448	0.4720	0.4720	0.0272
Glu	0	0	1.7714	1.6855	0.0769	0.7991	0.7991	0.0445
Lac	0	0	0.5216	1.0083	0.1747	0.4047	0.4047	0.0001
GABA	5	0.2500	2.5924	4.2107	0.2030	4.6468	4.6468	0.0097

a) GABA Solution

	Actual Concentration (mM)	Actual Standard Deviation (%)	1x1x1cm ³ Voxel Concentration (mM)	1x1x1cm ³ Standard Deviation (%)	1x1x1cm ³ P-Value (T-test)	1x1x2cm ³ Voxel Concentration (mM)	1x1x2cm ³ Standard Deviation (%)	1x1x2cm ³ P-Value (T-test)
NAA	12.5	0.6250	5.1157	3.0372	0.1044	9.9167	2.7136	0.0535
Cr	10	0.5000	3.6824	2.9065	0.2235	7.4346	1.4286	0.2543
Cho	3	0.1500	4.0060	6.3993	0.4896	2.2911	0.2356	0.0000
ml	7.5	0.3750	2.8587	0.4838	0.4451	5.3932	3.0221	0.1285
Glu	13	0.6250	3.1550	2.3865	0.2055	14.060	2.9264	0.2390
Lac	5	0.2500	0.3300	0.5856	0.4579	3.1210	0.8841	0.0518
GABA	0	0	1.8266	1.3077	0.1064	0.4088	0.7303	0.0517

b) BRAINO Solution

	Actual Concentration (mM)	Actual Standard Deviation (%)	1x1x1cm ³ Voxel Concentration (mM)	1x1x1cm ³ Standard Deviation (%)	1x1x1cm ³ P-Value (T-test)	1x1x2cm ³ Voxel Concentration (mM)	1x1x2cm ³ Standard Deviation (%)	1x1x2cm ³ P-Value (T-test)
NAA	12.5	0.6250	11.831	0.3727	0.0004	12.607	0.4509	0
Cr	10	0.5000	12.943	1.1783	0.0017	10.481	1.0280	0.0516
Cho	3	0.1500	2.5826	0.7164	0.0416	2.7792	0.2779	0.0025
ml	7.5	0.3750	3.8435	3.3922	0.0694	7.7397	0.8346	0.0021
Glu	13	0.6250	11.060	5.1107	0.1248	12.032	1.2352	0.0512
Lac	5	0.2500	4.0676	2.0802	0.1356	4.5931	0.9341	0.0499
GABA	10	0.5000	6.5579	4.8154	0.0846	10.491	2.3651	0.0037

c) BRAINO+GABA Solution

FIGURE 4.2: The 2 tailed type 3 T-test results for the GABA, BRAINO, and BRAINO+GABA solutions using the PRESS sequence are represented here. The actual and estimated concentrations by TARQUIN along with respective standard deviations are shown. The P-value result of the T-test comparing estimated vs. actual concentrations for each metabolite are also shown. Measurements were conducted within 1x1x1cm³ (left-most columns) and 1x1x2cm³ voxels (right-most columns). Figures a), b), and c) show all of the statistical values in GABA, BRAINO, and BRAINO+GABA solutions respectively.

Analysis of the BRAINO-only solutions reflected more accurate measurements than the GABA-only solutions, in the $1 \times 1 \times 2 \text{cm}^3$ acquisition voxel ($n=7$). In the $1 \times 1 \times 1 \text{cm}^3$ voxel ($n=7$), no metabolites were properly estimated as it can be further established that this voxel size paired with the contents of BRAINO is not an appropriate measure within the TARQUIN software package. As mentioned, the $1 \times 1 \times 2 \text{cm}^3$ voxel yielded better results, however, could only properly estimate the concentration of the GABA metabolite within both an appropriate concentration window and a p-value below 0.05. Although some metabolites had p-values under 0.05, their concentration estimates were far from the actual concentrations found in the BRAINO solution.

Analysis of the BRAINO+GABA solutions reflected much more accurate measurements compared to the above solutions regarding all metabolites including GABA. The NAA, Cr, and Cho metabolites were found to be accurate and repeatable with standard deviations below 1.2% and p-values below 0.5 in the $1 \times 1 \times 1 \text{cm}^3$ voxel ($n=7$). The GABA metabolite was not accurately measured in the $1 \times 1 \times 1 \text{cm}^3$ voxel where TARQUIN estimated the concentration of GABA to be 6.6mM compared to the actual 10mM, assessed a high standard deviation of 4.8% and a poor p-value of 0.0846. In the $1 \times 1 \times 2 \text{cm}^3$ voxel ($n=7$), all metabolites were estimated appropriately with reasonable standard deviations (i.e. $<1.3\%$ and $p < 0.05$). All metabolites, including GABA, were appropriately estimated concluding that, similar to LCMoDel, TARQUIN requires an increase in volume to accurately assess concentrations in neuronal-type solutions such as BRAINO+GABA.

4.4.2 TARQUIN analysis of the MEGA-PRESS sequence

The next analysis step was determination of metabolite concentrations from TARQUIN for the 7 phantom scanning sessions using MEGA-PRESS. Results are shown in Figure 4.3. It was noted that TARQUIN provided reliable estimates of GABA within all solutions, within the $1 \times 1 \times 2 \text{cm}^3$ acquisition voxels. This was statistically assessed using a

2-tailed T-test comparing actual concentrations with estimates from TARQUIN. Measurements were also rejected if the FWHM was under 4Hz, therefore only $1 \times 1 \times 1 \text{cm}^3$ and $1 \times 1 \times 2 \text{cm}^3$ voxels were used. Finally, for the following measurements, only the NAA and GABA concentrations can be estimated as the MEGA-PRESS sequence is specified to measure GABA as the metabolite of interest and NAA as a reference metabolite.

Analysis of the GABA-only solution yielded convincing results regarding NAA in the $1 \times 1 \times 1 \text{cm}^3$ and $1 \times 1 \times 2 \text{cm}^3$ voxels. More accurate measurements were found in the $1 \times 1 \times 2 \text{cm}^3$ voxel with decreased standard deviations and lower p-values. GABA concentration was only appropriately estimated within the $1 \times 1 \times 2 \text{cm}^3$ voxel with a standard deviation of 1.2% and a p-value of 0.0280. Basis sets within TARQUIN for MEGA-PRESS were therefore reliable for further GABA-only measurements as long as a voxel volumes above 2cm^3 are to be employed.

Results of the BRAINO-only solutions were not as straight forward compared to the GABA-only solution. For example, in BRAINO-only, NAA was only accurately measured in the $1 \times 1 \times 1 \text{cm}^3$ voxel, whereas in the $1 \times 1 \times 2 \text{cm}^3$ voxel a p-value of 0.1780 was determined. With regards to GABA, the BRAINO-only solution appropriately estimated 0mM ($p < 0.05$) for both voxel sizes. Although this experiment did not provide confidence in the NAA measurement, the GABA estimation remained accurate and should be considered for further investigation, similar to results obtained using LCModel.

Analysis of the BRAINO+GABA solutions reflected similar observations as seen in LCModel. The $1 \times 1 \times 1 \text{cm}^3$ voxel yielded poor and non-repeatable results for NAA along with a poor estimation of GABA. In the $1 \times 1 \times 2 \text{cm}^3$ voxel, NAA was appropriately measured, however not quite significant (p-value=0.0818). GABA was accurately measured

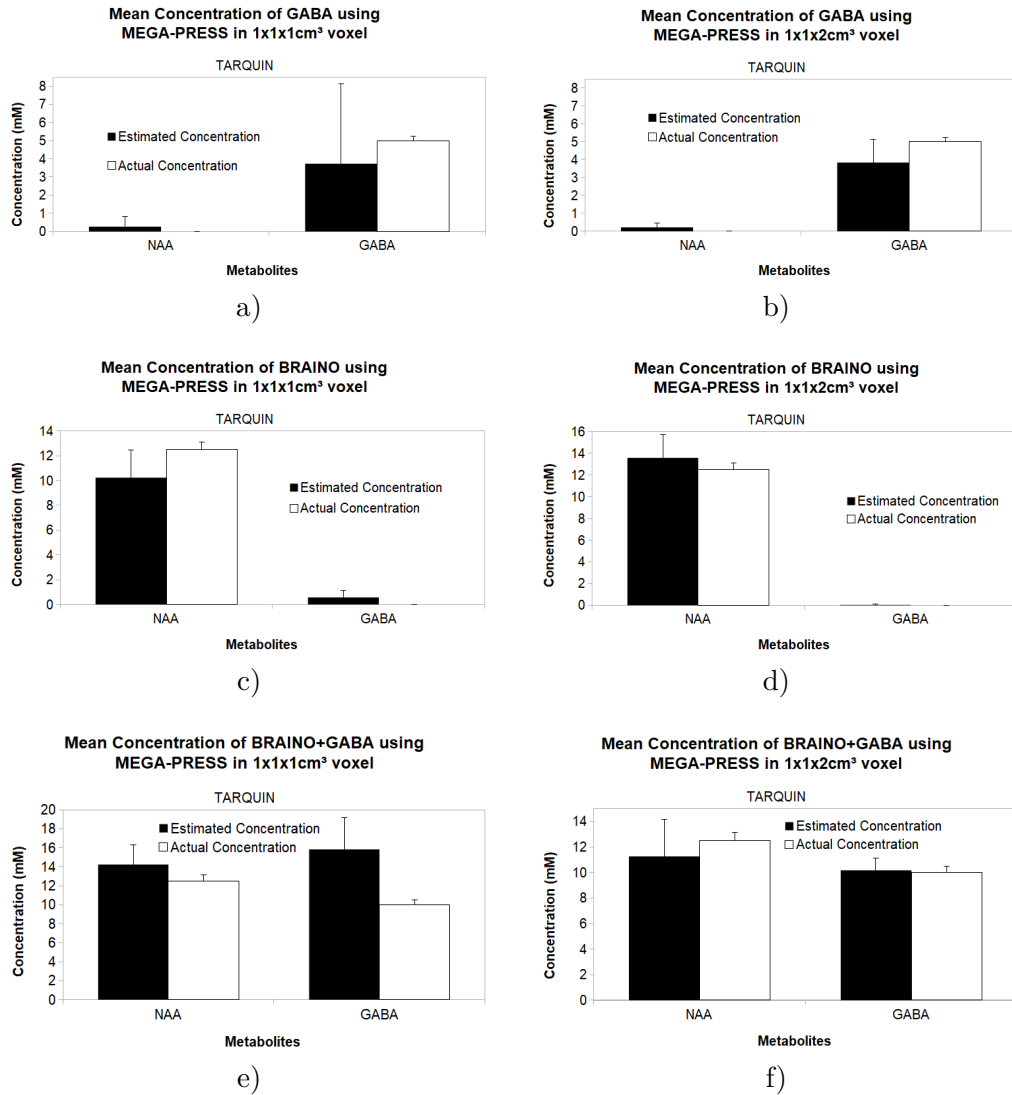


FIGURE 4.3: Graphical representation of the mean concentrations of metabolites found in GABA, BRAINO, or BRAINO+GABA solutions using the MEGA-PRESS sequence in a selected voxel size (i.e. 1x1x1cm³ or 1x1x2cm³). The mean (n=7) estimated concentrations by TARQUIN of metabolites (NAA and GABA) are shown in black, whereas the actual concentrations are shown in white. Positive standard deviations are also represented by black error bars. Figures a), c), and e) show concentrations within a selected 1x1x1cm³ voxel for GABA, BRAINO, and BRAINO+GABA solutions respectively. Figures b), d), and f) show concentrations within a selected 1x1x2cm³ voxel for GABA, BRAINO, and BRAINO+GABA solutions respectively.

	Actual Concentration (mM)	Actual Standard Deviation (%)	1x1x1cm ³ Voxel Concentration (mM)	1x1x1cm ³ Standard Deviation (%)	1x1x1cm ³ P-Value (T-test)	1x1x2cm ³ Voxel Concentration (mM)	1x1x2cm ³ Standard Deviation (%)	1x1x2cm ³ P-Value (T-test)
NAA	0	0	0.2661	0.5414	0	0.2268	0.2198	0
GABA	5	0.2500	3.7322	4.3948	0.1902	3.8425	1.2952	0.0280

a) GABA Solution

	Actual Concentration (mM)	Actual Standard Deviation (%)	1x1x1cm ³ Voxel Concentration (mM)	1x1x1cm ³ Standard Deviation (%)	1x1x1cm ³ P-Value (T-test)	1x1x2cm ³ Voxel Concentration (mM)	1x1x2cm ³ Standard Deviation (%)	1x1x2cm ³ P-Value (T-test)
NAA	12.5	0.6250	10.238	2.1973	0.0006	13.580	2.1016	0.1780
GABA	0	0	0.5756	0.5365	0.0023	0.0354	0.0868	0.0333

b) BRAINO Solution

	Actual Concentration (mM)	Actual Standard Deviation (%)	1x1x1cm ³ Voxel Concentration (mM)	1x1x1cm ³ Standard Deviation (%)	1x1x1cm ³ P-Value (T-test)	1x1x2cm ³ Voxel Concentration (mM)	1x1x2cm ³ Standard Deviation (%)	1x1x2cm ³ P-Value (T-test)
NAA	12.5	0.6250	14.238	2.0915	0.1170	11.269	2.9050	0.0818
GABA	10	0.5000	15.825	3.3399	0.0026	10.179	0.9691	0.0151

c) BRAINO+GABA Solution

FIGURE 4.4: The 2 tailed T-test results for the GABA, BRAINO, and BRAINO+GABA solutions using the MEGA-PRESS sequence are represented here. The actual and estimated concentrations by TARQUIN along with respective standard deviations are shown. The P-value result of the T-test comparing estimated vs. actual concentrations for each metabolite (NAA and GABA) are also shown. Measurements were conducted within 1x1x1cm³ (left-most columns) and 1x1x2cm³ voxels (right-most columns). Figures a), b), and c) show all of the statistical values in GABA, BRAINO, and BRAINO+GABA solutions respectively.

in the 1x1x2cm³ voxel, with an estimated concentration of 10.18mM and standard deviation less than 1% (p-value = 0.0151). The BRAINO+GABA solution estimates using TARQUIN provided reliable, repeatable, and accurate measurements for future GABA investigation, again with the caveat that the voxel is at least 2cm³ in volume.

4.4.3 TARQUIN and LCModel software comparison

The final software assessment was to determine whether results of TARQUIN and LCModel were similar. Results are displayed in Table 4.5. Although similar conclusions can be made regarding the outcomes from both software types, the only characteristic they share consistently is the estimation of GABA within a $1 \times 1 \times 2 \text{cm}^3$ acquisition voxel. With the PRESS sequence, most metabolites in the BRAINO and BRAINO+GABA solutions appeared similar. However, a few metabolites had p-values higher than 0.05 which lends towards poor similarities within softwares. MEGA-PRESS had similar findings in

	GABA solution		BRAINO Solution		BRAINO+GABA Solution	
	1x1x1cm ³ Voxel P-Value (Ttest)	1x1x2cm ³ Voxel P-Value (Ttest)	1x1x1cm ³ Voxel P-Value (Ttest)	1x1x2cm ³ Voxel P-Value (Ttest)	1x1x1cm ³ Voxel P-Value (Ttest)	1x1x2cm ³ Voxel P-Value (Ttest)
NAA	0.1214	0.4445	0.1588	0.0742	0.0010	0.0000
Cr	0.0001	0.2890	0.1532	0.0000	0.0494	0.1843
Cho	0.0744	0.2532	0.3490	0.0000	0.0028	0.0001
ml	0.1856	0.2780	0.4177	0.1099	0.2075	0.0033
Glu	0.1468	0.1594	0.1184	0.3552	0.0242	0.0089
Lac	0.1797	0.0008	0.4153	0.0364	0.0866	0.1395
GABA	0.0532	0.0011	0.4617	0.0146	0.1220	0.0089

a) PRESS Software Comparison

	GABA solution		BRAINO Solution		BRAINO+GABA Solution	
	1x1x1cm ³ Voxel P-Value (Ttest)	1x1x2cm ³ Voxel P-Value (Ttest)	1x1x1cm ³ Voxel P-Value (Ttest)	1x1x2cm ³ Voxel P-Value (Ttest)	1x1x1cm ³ Voxel P-Value (Ttest)	1x1x2cm ³ Voxel P-Value (Ttest)
NAA	0.2582	0.2985	0.1746	0.0619	0.1538	0.1561
GABA	0.2525	0.0661	0.4477	0.0920	0.0126	0.0188

b) MEGA-PRESS Software Comparison

FIGURE 4.5: The table shows P-values generated from a 2 tailed T-test performed comparing estimated concentrations from both LCModel and TARQUIN software packages. Each respective metabolite was investigated for all three solution types (GABA, BRAINO, BRAINO+GABA) along with each voxel dimension ($1 \times 1 \times 1 \text{cm}^3$ and $1 \times 1 \times 2 \text{cm}^3$). Figure a) demonstrates P-value results for PRESS, while Figure b) shows P-values for MEGA-PRESS.

that NAA was only similar within the BRAINO solution and the GABA metabolite measurements are consistent in the $1 \times 1 \times 2 \text{cm}^3$ acquisition voxel for each solution.

Chapter 5

In vivo Measurements of B_0 and B_1^+ Variations as Confounders in ^1H -MRS

5.1 Rationale

In vivo ^1H -MRS is very difficult to perform well and quickly. First, the metabolites of interest are on the order of 10000x smaller than the dominant water resonance (55M). Hence the technique is highly SNR limited. Furthermore, physiological motion and also susceptibility (i.e. bone/tissue or air/tissue interfaces) artifacts add other difficult complexities. Susceptibility differences lead to inhomogeneity in the main magnetic field (B_0) and also variations in the transmit RF field (B_1^+). In the cervical spinal cord motion is complex and due to cardiac contractility, respiratory motion induced by the lungs, and pulsatile flow motion induced by vertebral arteries and CSF around the spinal cord (Henning, 2008). Although there have been techniques to reduce this noise such as ECG triggering and spectral outer volume suppression (OVS), these techniques have shown negligible improvements for cervical spinal cord (Hock, 2013). Either signal

boosting or noise reduction methods are often attempted to increase the SNR in this area ^1H -MRS data.

One approach that may lead to significant improvements in spectral quality includes applying corrections for B_0 and B_1^+ . Reduction in inhomogeneity of both indicate improved MR quality. Their variability is often associated with motion. To date, there have not been any comprehensive assessments of temporal changes in B_0 and B_1^+ , in cervical spinal cord. Thus the goal of this experiment was correlate physiologic motion (cardiac and respiratory) with temporal changes in B_0 and B_1^+ variability during the length of a typical MEGA-PRESS scan (i.e. for GABA).

5.2 Hypotheses

This experiment was designed to investigate the relationship between physiological data (i.e. pulsatile flow and respiratory motion) and the variation between acquired B_0 and B_1^+ fields at the level of C4 in the spinal cord. It was hypothesized that temporal fluctuations in these MR calibration metrics would correlate temporally with cardiac and/or respiratory waveforms.

5.3 Methods

5.3.1 Participants

In vivo ^1H -MRS was performed in ten healthy human participants (6 males, mean age 25.9 years, SD \pm 9.14 and 4 females, mean age 23.5 years, \pm 0.58). Healthy participants were recruited with the focus being on males and females between the ages of 18 and 45, inclusive. Recruitment was facilitated through advertisements posted within

St. Joseph's Healthcare (Charlton Campus). The participant exclusion criteria included contraindications for an MRI scan (claustrophobia, implanted devices, permanent piercings) along with refraining from alcohol, nicotine, and non-prescription drugs in the 12 hours prior. The study was approved by the Hamilton Integrated Research Ethics Board (HiREB).

5.3.2 ^1H -MRS Sequences and Protocols

All MRI/MRS was performed using a GE MR750 3 Tesla MRI system (General Electric Healthcare, Milwaukee WI) and a 32 channel Head-Neck-Spine (HNS) plus brachial coil array RF. An integrated body-coil was used for RF transmission (GE Head Neck and Spine coil). MR scanning included the following four sequences :

- 3-plane localizer scan (steady-state fast spine echo (SSFSE) with TE/TR = 81.1/800 ms) for positioning of ^1H -MRS voxels and prescribing acquisition planes for B_0 and B_1^+ field maps.
- ~10 minute MEGA-PRESS scan (TE/TR = 68/2000 ms, NEX = 320), positioning the top of a $1 \times 1 \times 2 \text{cm}^3$ acquisition voxel flush to the inferior aspect of the C4 vertebral body.
- ~10 minutes B_0 dynamic field mapping scan (TE/TR = 4.60/31.4 ms, FOV = 24, slice thickness = 3mm), positioning the scanning plane in the transverse direction flush to the inferior aspect of the C4 vertebral body. B_0 dynamic field maps are produced every 8 seconds, therefore 75 B_0 field maps were generated over the 10 minute scanning session.
- ~10 minute B_1^+ dynamic field mapping scan (TE/TR = 13.9/20.0 ms, FOV = 24, slice thickness = 3mm), positioning the scanning plane in the transverse direction

flush to the inferior aspect of the C4 vertebral body. B_1^+ dynamic field maps are produced every 6 seconds, therefore 100 B_1^+ field maps were generated over the 10 minute scanning session.

All MR sequences were accompanied by collection of physiological data acquisition hardware setup prior to the beginning of scanning. Physiological measurements were recorded concurrently with all 4 MR sequences. Pulsatile flow and respiratory motion were recorded over each entire scan at a sampling rate of 10Hz and 25Hz, respectively, using the GE MR control variable `phys_record_flag`. Pulsatile flow data was acquired using a pulse oximeter (Figure 5.1) placed on the right index finger of participants. A pulse oximeter is a non-invasive MR-compatible instrument that uses infrared light to detect blood oxygen saturation. The signal intensity from a pulse oximeter is directly proportional to an individual's blood oxygen saturation. This value fluctuates with the cardiac cycle. Hence pulsatile flow is inferred from temporal fluctuation in oxygen saturation. In addition to pulse oximetry, respiratory motion was digitized over the course of each MR sequence, acquired using a thoracic respiratory bellows (Figure 5.1). A thoracic

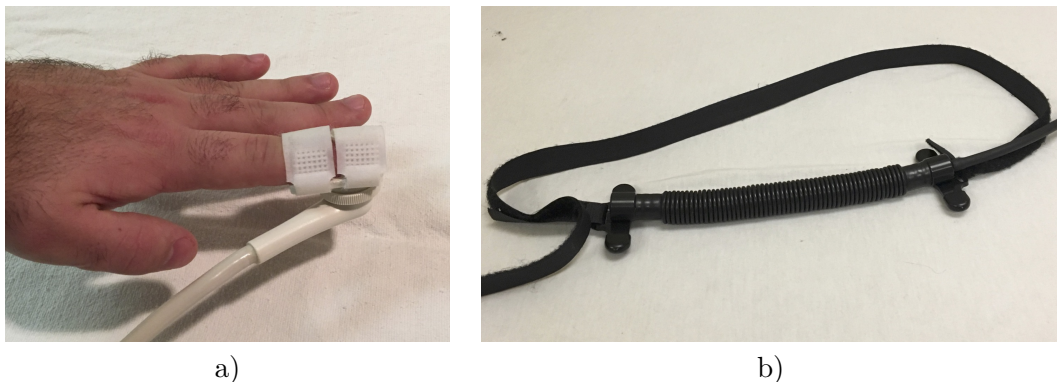


FIGURE 5.1: a) A pulse oximeter was placed on the index finger of each individual to measure pulsatile flow. b) A thoracic respiratory bellows, that wraps around the mid-abdomen to measure respiratory motion data. This pneumatic device uses a pressure transducer that is activated based on pressure changes within the respiratory bellows.

respiratory bellows is a non-invasive MR-compatible instrument that measures changes in breathing. An influx in signal intensity of a thoracic respiratory bellows is equivalent to passive inspiration, whereas efflux in signal intensity represents expiration. The thoracic respiratory bellow tool can therefore calculate the rhythmic breathing pattern of an individual.

Healthy human subjects were scanned in addition to the spinal cord phantom, mentioned in previous chapters, to ensure B_0 and B_1^+ were not changing significantly in a controlled and motionless environment. The B_0 and B_1^+ field map sequences were auto-shimmed only once at the beginning of each scan to maintain the same shim for the duration of the 10 minute scan.

5.3.3 Analysis Pipeline

For the analysis, 10 scanning sessions were collected from phantoms and healthy adult subjects. The data analysis pipeline began with selecting a $1 \times 1 \text{cm}^2$ ROI in the B_0 and B_1^+ field maps. The ROI was selected within each map, over time, for each subject. The ROI geometry was selected to be as close to the MRS acquisition voxel as possible. The acquisition voxel dimensions selected for the MEGA-PRESS scan is shown in a phantom and a human subject (Figure 5.2). For phantom measurements, the ROI was placed centered within a tube of interest, whereas within subjects, an ROI was centered within the cervical spinal cord level C4.

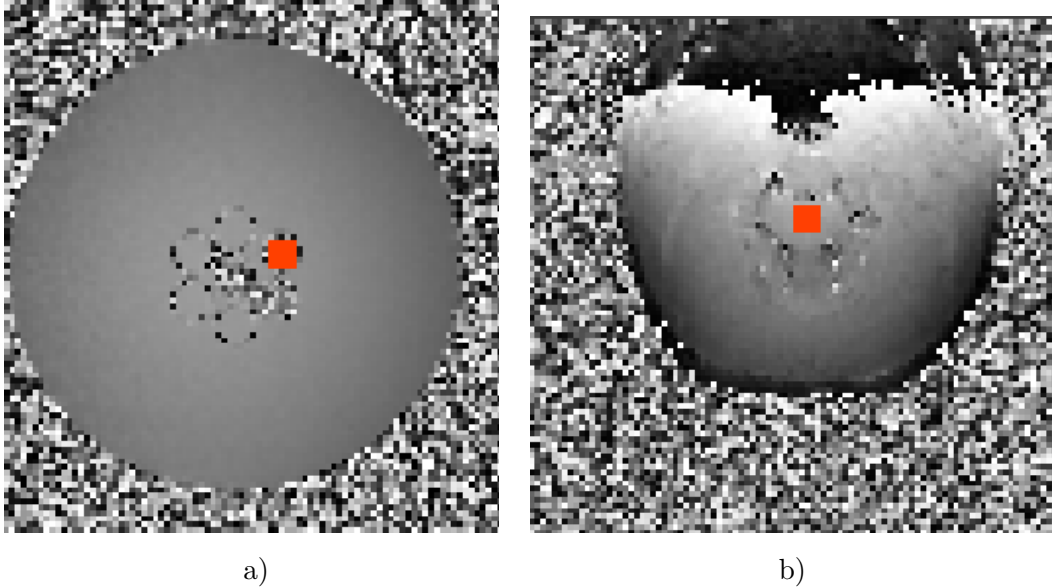


FIGURE 5.2: a) a B_0 field map representing the selected ROI in red within the phantom. b) a B_0 field map representing the selected ROI in red within a healthy human subject.

Next, the mean change over time within ROIs were calculated. ROIs in the phantom and human subjects were calculated over a field-of-view (FOV) of 24cm and over a 10-minute timespan.

Physiological data was analyzed to identify significant frequency contributions from pulsatile and respiratory flow. Data for pulsatile flow (PPG) was collected over the 10-minute duration of the repeated B_0 and B_1^+ field map scans. PPG data was processed for every field map, where data underwent a Fourier Transform (FT) and Power Spectral Density (PSD) calculation to obtain a frequency signature of the PPG data. As 75 B_0 and 100 B_1^+ field maps were generated over 10 minutes, 75 and 100 PPG PSD's were therefore obtained, respectively. Lastly, the magnitude for each PSD was calculated to identify the global frequency contributions for each field map. An example of the results for the B_0 PPG PSD magnitudes for one healthy adult subject are shown in Figure 5.3 a).

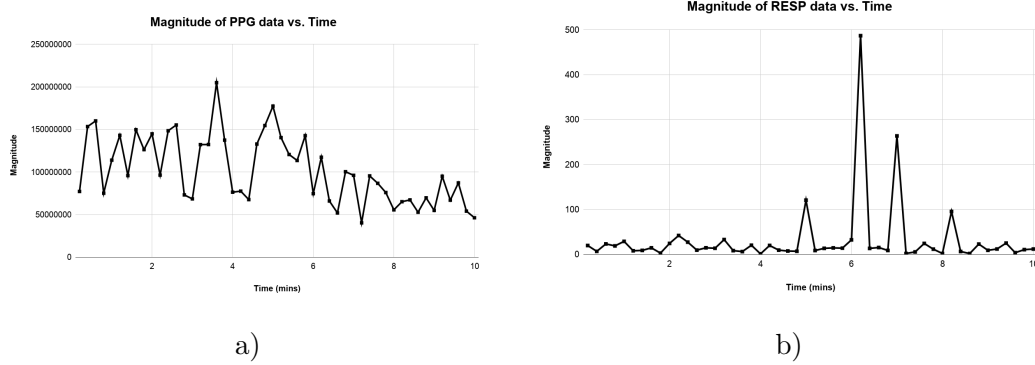


FIGURE 5.3: a) PPG PSD magnitudes for each B_0 field map for one scanning session. The time represents when each PSD magnitude was calculated (i.e. every 6 seconds) b) RESP data magnitude for each B_0 field map for one scanning session. The time represents when each RESP magnitude was calculated (i.e. every 6 seconds).

Data for human respiratory data (RESP) was also collected over the 10-minute duration of the repeated B_0 and B_1^+ field map scans. As RESP data has a significantly lower frequency than PPG data, a sliding standard deviation window was used to calculate a unique human respiratory rhythm pattern for each subject. As 75 B_0 and 100 B_1^+ field maps were generated over 10 minutes, 75 and 100 RESP sliding standard deviation windows were therefore obtained, respectively. An example of the results for the B_0 RESP sliding standard deviation windows for one healthy adult subject are shown in Figure 5.3 b).

PPG and RESP data were further evaluated and compared with ΔB_0 and ΔB_1^+ . Data normality was determined through assessment of kurtosis and skewness (also performed a Jarque-Bera test, which tests both the 3rd and 4th moment about the mean as a combined binary metric). Principal component analysis (PCA) was performed to determine whether physiological variations (PPG and RESP) significantly contributed to the variance in B_0 and B_1^+ fields. The primary PCA components were PPG, RESP, and ΔB_0 and/or ΔB_1^+ (depending on which MR element was under investigation). Finally, correlation analysis was performed between combinations of PPG, RESP, ΔB_0 , and ΔB_1^+ to identify how the physiological motion and/or noise affects MRI field maps

and thus data quality.

5.4 Results and Discussion

The ΔB_0 and ΔB_1^+ parameters were first calculated in the phantom yielding a ΔB_0 (mean \pm SD) of 0.47 ± 0.51 ppm and a ΔB_1^+ of 28.4 ± 0.272 °/flip angle. The ΔB_0 and ΔB_1^+ were also calculated in the healthy adult subjects yielding a ΔB_0 of 0.38 ± 2.7 ppm and a ΔB_1^+ of 21.4 ± 4.61 °/flip angle. This confirms that although the average change over time is similar comparing the phantom and the subjects, the standard deviation is significantly higher (fourfold in ΔB_0 and twofold in ΔB_1^+) in healthy subjects compared to the phantom.

Upon acquiring the processed PPG and RESP data, principle component analysis (PCA) was performed. The results are shown in Figure 5.4 The principle components in B_0 included PPG, RESP, and ΔB_0 magnitudes. The largest source of variance was attributed to PPG (total variance explained 41.43%), and the second largest component was attributed to RESP (total variance explained 35.05%). For ΔB_1^+ PCA showed the greatest source of variance was RESP (total variance explained 47.27%), with the second largest component being attributed to PPG (39.99%). Thus PCA analysis validates that frequency magnitude characteristics of both PPG and RESP contribute to noise in the B_0 and B_1^+ field maps.

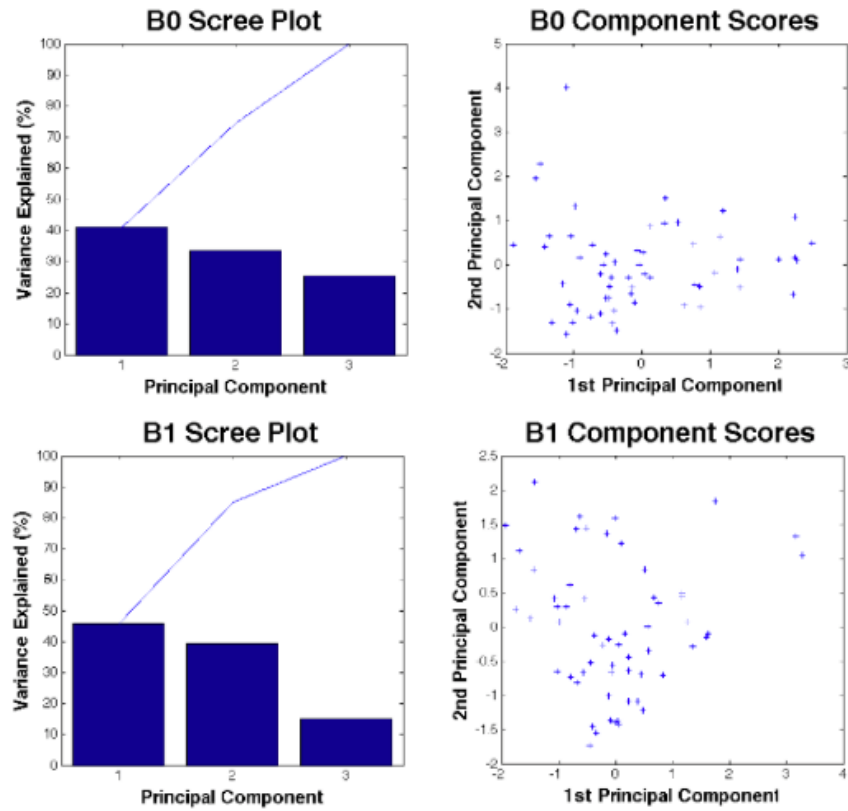


FIGURE 5.4: Principle component analysis (PCA) was performed to find the principle contributors to noise in the ΔB_0 and ΔB_1^+ measurements. Scree plots show 3 principle components where in B_0 , the first, second, and third principle components were PPG, RESP, and ΔB_0 respectively; and in B_1^+ , the first, second, and third principle components were RESP, PPG, and ΔB_1^+ . Component scores also demonstrate how the primary and secondary components are correlated (i.e. RESP and PPG in both cases) and how they contribute towards affecting noise in the B_0 and B_1^+ field maps.

As PCA confirmed that PPG and RESP contribute to variance in ΔB_0 and ΔB_1^+ over time, a correlation analysis was performed (Figure 5.5) detailing how PPG and RESP correlate to ΔB_0 and ΔB_1^+ respectively.

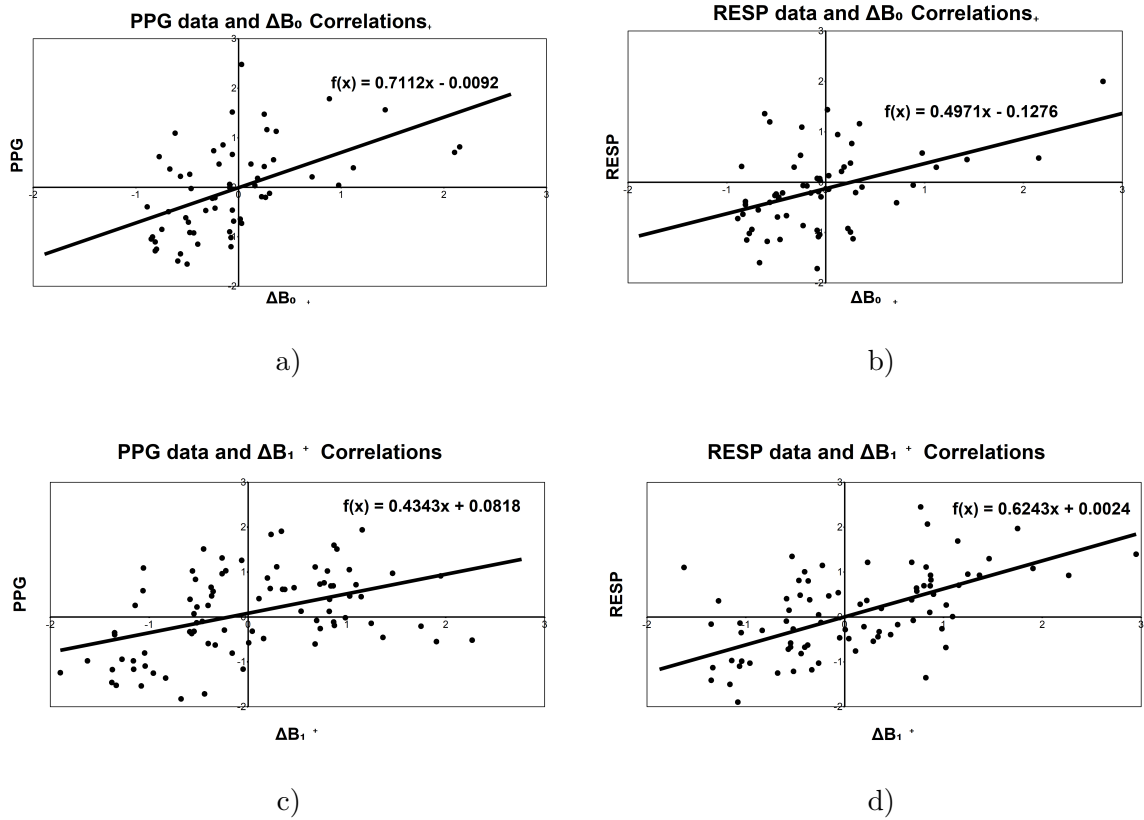


FIGURE 5.5: Correlation Analysis was performed to identify relationships between physiological motion measures (PPG and RESP) and the ΔB_0 and/or ΔB_1^+ . Figures a) and b) demonstrate the correlation plots and equations between physiological motion measures and ΔB_0 . Figure a) shows the PPG and ΔB_0 correlative relationship while Figure b) shows the RESP and ΔB_0 correlative relationship. Figures c) and d) focus on ΔB_1^+ . Figure c) shows the PPG and ΔB_1^+ correlative relationship while Figure d) shows the RESP and ΔB_1^+ correlative relationship.

For the correlation analysis two relationships yielded a correlation coefficient (R^2) above 0.5. The most significant relationships were found between PPG data and ΔB_0 , yielding a correlation coefficient of 0.71 ($R^2 = 0.3905$, $F = 0.00024$) and between RESP and ΔB_1^+ , yielding a correlation coefficient of 0.62 ($R^2 = 0.2621$, $F = 0.00507$). As PCA identified the principle components affecting variability within the ΔB_0 and ΔB_1^+ measurements, the principle component in ΔB_0 (PPG) in fact correlates strongly with

the variation in ΔB_0 . The same can be said regarding the principle component in ΔB_1^+ as RESP had the most significant correlation amongst all other components.

Chapter 6

Conclusions and Future Work

6.1 Summary of Findings

^1H -MRS is an useful tool for investigating the contents of neuronal tissue. However, there are a number of challenges when translating this technique to the spinal cord. Therefore reliable tools need to be developed to maximize accuracy and precision of data collection. Major findings in this work include the simulation of ^1H -MRS in a spinal cord phantom, a comparison of reliability and repeatability of commonly used software platforms, and finally the discovery of a possible noise reduction technique for in vivo acquisition.

6.1.1 Experiment 1

In this experiment LCModel provided reliable spectral analysis and concentration estimations of GABA. However, it was found that a voxel size of $1 \times 1 \times 2 \text{cm}^3$ is ideal. Any larger and the acquisition suffers from poor shim, and hence poor reliability. Any smaller and the acquisition suffers from reduced SNR (i.e. SNR is proportional to acquisition voxel volume).

For phantom studies differences between PRESS and MEGA-PRESS sequences in estimating the concentration of GABA were not completely clear. Although MEGA-PRESS allowed more accurate estimation of GABA, the reference NAA concentration had significant deviations and fluctuations leading to questions whether GABA estimation was correct. Finally, PRESS can offer fairly repeatable measures of other metabolites. Therefore the sequence should always be employed to measure metabolites other than GABA.

When using LCModel, it should be noted that the basis sets are very important as they must be appropriate for your metabolites of interest. When analyzing GABA-only, BRAINO-only, and BRAINO+GABA solutions, there were often some discrepancies found within some of the higher concentration metabolites such as NAA, Cr, and Glu. This problem can be associated with the higher degree of variance due to a larger volume, however, may possibly be accommodated by an improved spectral basis set.

To conclude, using the PRESS and MEGA-PRESS sequences, the mean concentration of GABA estimated by LCModel was similar to the true concentration, meaning the sequences, software tools, and voxel positioning and size combine for a reliable method of data acquisition for small voxels and spinal cord geometries.

6.1.2 Experiment 2

In this experiment, TARQUIN was shown to provide similar and reliable spectral analysis and concentration estimations of GABA compared to LCModel. As in Experiment 1, a voxel size of at least $1 \times 1 \times 2 \text{cm}^3$ must be used for TARQUIN analysis to converge on an appropriate estimation for metabolite concentrations.

Most conclusions from Experiment 1 overlap with Experiment 2, however some key differences should be noted. For example, TARQUIN did not accurately estimate the

GABA-only and BRAINO-only solutions. Therefore it is suggested the standard basis sets for TARQUIN could do with being improved to increase reliability of its measurements. It should be noted that BRAINO metabolites within TARQUIN may have an offset amongst its basis sets as the estimated concentrations for BRAINO metabolites were often underestimated.

When comparing TARQUIN to LCModel, there were some differences amongst metabolites such as NAA, mI, and Glu. However, a key finding was that GABA measurements in both software platforms were highly comparable, solidifying the idea that either software package can be equally as reliable and thus used to investigate GABA with ^1H -MRS.

To conclude, using PRESS and MEGA-PRESS sequences, the mean concentration of GABA estimated by TARQUIN was similar to the true concentrations and estimations by the LCModel software, meaning that the sequences, software tools, and voxel selection combine for a conclusive method of data acquisition for small voxel and spinal geometries.

6.1.3 Experiment 3

There were significant links between physiological data and B_0 and B_1^+ inhomogeneities within the spinal cord. ^1H -MRS approaches should continue to employ gating techniques to reduce detrimental effects caused by physiology. As investigated in this experiment, physiological motion characterized by pulsatile flow (PPG) and respiratory flow (RESP) of an individual was recorded and data acquired was transformed to describe the relationship that exists between physiological motion and B_0 and B_1^+ changes. Correlative relationships were found, as a correlation between PPG and RESP data was demonstrated. Although not completely significant, this information could lead to development of a difference equation that is able to subtract physiological motion from data collections thereby improving spectral quality. A significant area where this may be effective

is within PPG data and ΔB_0 along with RESP data and ΔB_1^+ .

6.2 Current Challenges and Future Work

In the context of this study there are a few areas that could be the focus of future experiments. Based on phantom analysis, future work should pursue embedding tubes within the phantom in a bone-mimicking encasement to assess potential problems with magnetic susceptibility and tissue-tissue boundaries. Although it was confirmed that GABA can be assessed within a controlled phantom environment, a study should be conducted to investigate the effects of different tissues on concentration estimates. In addition, to design a more robust and life-like phantom, flow should be introduced in the transverse and superior-inferior directions to mimic CSF and aortic blood flow artifacts. A study like this could better emulate spinal cord MR spectroscopy environments and further identify more convincing trends and correlations dependent on motion.

Further exploration into the relationship between the B_0 and B_1^+ magnetic field changes and respiratory/cardiac motion are also needed to more properly establish a difference equation that can reduce physiological noise within spinal cord data acquisition. Adding parameters to the analysis such as a larger sample size, analysis amongst different slice positions, and more component variables such as temperature, shim, and MR noise can help contribute to future work that can identify more convincing correlations. In addition, a more stringent population homogeneity may be warranted to further investigate how different ages and sexes in healthy individuals may affect the changes in B_0 and B_1^+ .

The work and research found in this MASc provided significant breakthroughs in improving and understanding ^1H -MRS within the cervical spinal cord. However, there remains a lengthy series of improvements that must be made before attempting this

technique for clinical and investigative purposes. As this research has demonstrated that this technique can be performed reliably in a controlled phantom environment, the introduction of various noise artifacts in vivo, still must be addressed. Extensive work remains to be performed in order to eliminate noise induced by the in vivo experiments and qualify this technique for reliable clinical use.

Appendix A

MATLAB Code

The following MATLAB codes were useful in data manipulation with regards to B_0 , B_1^1 , PPG, and RESP data.

This first function 'winny' was utilized to ensure that all arrays for the PPG and RESP windows were the same size for further array analysis :

```
function [ winny ] = winny( array1, i )
winny = array1(end-5-i:end-i);
end
```

The function 'splitter' was used to split the arrays for the PPG and RESP data in half to further evaluate the PPG and RESP data at the proper time periods :

```
function [ array1,array2 ] = splitter( testarray )
half = size(testarray)/2;
array1 = testarray(1:half);
array2 = testarray(half+1:end);
end
```

The function `outdex` nested the `winny` function in order to generate the proper PPG and RESP data index to further FFT and PSD the physiological data :

```
function [ q ] = outdex(array1,array2,trunc)
winny = zeros(size(array1));
for i = 1:6
    winny(i) = array1(end-6-trunc+i);
end

[resultat] = ismember(array2,winny);
[outdexe] = find(resultat)
p = find(diff(outdexe)==1);
p2 = find(diff(p)==1);
p3 = find(diff(p2)==1);
p4 = find(diff(p3)==1);
p5 = find(diff(p4)==1);
q5 = p4(p5(1));
q4 = p3(q5);
q3 = p2(q4);
q2 = p(q3);
q = outdexe(q2+5);
```

Appendix B

Bash Script Code

The following Bash code was useful to analyze TARQUIN P-file data :

```
#!/bin/bash

echo " "
echo -n "Name the PFile : "
read pfile

# dref_signals 1h_cr_cho \
# dref_signals 1h_h2o \
# int_basis braino \
# int_basis megapress_gaba \

cd/Applications
./tarquin --input ~/Desktop/$pfile \
  --pul_seq press
  --dyn_freq_corr true \
  --dyn_av all \
```

```
--dref_signals 1h_cr_cho \  
--ref 4.85 \  
--start_pnt 5 \  
--ref_signals 1h_naa \  
--int_basis braino \  
--w_conc 55556 \  
--w_att 0.7 \  
--output_csv ~/Desktop/${pfile}_PRESS.csv
```

Bibliography

Barantin, L., A. L. Pape, and S. Akoka (1997).

A new method for absolute quantitation MRS metabolites.

Magnetic resonance in medicine 38 (2):179–182.

Blicher, J. U., J. Near, E. Næss-Schmidt, C. J. Stagg, H. Johansen-Berg, J. F. Nielsen, L. Østergaard, and Y.-C. L. Ho (2015).

GABA levels are decreased after stroke and GABA changes during rehabilitation correlate with motor improvement.

Neurorehabilitation and neural repair 29 (3):278–286.

Cadotte, D. W., R. Bosma, D. Mikulis, N. Nugaeva, K. Smith, R. Pokrupa, O. Islam, P. W. Stroman, and M. G. Fehlings (2012).

Plasticity of the injured human spinal cord: insights revealed by spinal cord functional MRI.

PLoS One 7 (9):e45560.

Convento, S., C. Russo, L. Zigiotta, and N. Bolognini (2016).

Transcranial electrical stimulation in post-stroke cognitive rehabilitation.

European Psychologist.

De Graaf, R. A. (2013).

In vivo NMR spectroscopy: principles and techniques.

John Wiley & Sons.

De Leener, B., M. Taso, J. Cohen-Adad, and V. Callot (2016).

Segmentation of the human spinal cord.

BIBLIOGRAPHY

- Magnetic Resonance Materials in Physics, Biology and Medicine* 29 (2):125–153.
- Drost, D. J., W. R. Riddle, and G. D. Clarke (2002).
Proton magnetic resonance spectroscopy in the brain: report of AAPM MR Task Group# 9.
Medical physics 29 (9):2177–2197.
- El Masri, W. (2006).
Traumatic spinal cord injury: the relationship between pathology and clinical implications.
Trauma 8 (1):29–46.
- Fertikh, D. and M. Brooks (2006).
Multiple sclerosis, spine.
- Harada, M., M. M. Taki, A. Nose, H. Kubo, K. Mori, H. Nishitani, and T. Matsuda (2011).
Non-invasive evaluation of the GABAergic/glutamatergic system in autistic patients observed by MEGA-editing proton MR spectroscopy using a clinical 3 tesla instrument.
Journal of autism and developmental disorders 41 (4):447–454.
- Hashimoto, T., M. Tayaina, M. Miyazaki, E. Fujii, M. Harada, H. Miyoshi, M. Tannuchi, and Y. Kuroda (1995).
Developmental brain changes investigated with proton magnetic resonance spectroscopy.
Developmental Medicine & Child Neurology 37 (5):398–405.
- Heinzer-Schweizer, S., N. De Zanche, M. Pavan, G. Mens, U. Sturzenegger, A. Henning, and P. Boesiger (2010).
In-vivo assessment of tissue metabolite levels using ¹H MRS and the Electric Reference To access In vivo Concentrations (ERETIC) method.

BIBLIOGRAPHY

- NMR in Biomedicine: An International Journal Devoted to the Development and Application of Magnetic Resonance In vivo* 23 (4):406–413.
- Hellerbach, A., V. Schuster, A. Jansen, and J. Sommer (2013).
MRI phantoms—are there alternatives to agar?
PloS one 8 (8):e70343.
- Henning, A., M. Schär, S. S. Kollias, P. Boesiger, and U. Dydak (2008).
Quantitative magnetic resonance spectroscopy in the entire human cervical spinal cord and beyond at 3T.
Magnetic resonance in medicine 59 (6):1250–1258.
- Hock, A., E. L. MacMillan, A. Fuchs, R. Kreis, P. Boesiger, S. S. Kollias, and A. Henning (2013).
Non-water-suppressed proton MR spectroscopy improves spectral quality in the human spinal cord.
Magnetic resonance in medicine 69 (5):1253–1260.
- Kakulas, B. A. and C. Kaelan (2015).
The neuropathological foundations for the restorative neurology of spinal cord injury.
Clinical neurology and neurosurgery 129:S1–S7.
- Kearney, H., D. H. Miller, and O. Ciccarelli (2015).
Spinal cord MRI in multiple sclerosis—diagnostic, prognostic and clinical value.
Nature Reviews Neurology 11 (6):327.
- Kossowski, B., J. Orzeł, P. Bogorodzki, M. Wilson, Z. Setkiewicz, and S. P. Gazdzinski (2017).
Follow-up analyses on the effects of long-term use of high fat diet on hippocampal metabolite concentrations in Wistar rats: Comparing Tarquin quantification of 7.0 T rat metabolites to LCModel.
Biol 2 (4):1–7.

BIBLIOGRAPHY

- Lattanzi, R., A. K. Grant, J. R. Polimeni, M. A. Ohliger, G. C. Wiggins, L. L. Wald, and D. K. Sodickson (2010).
Performance evaluation of a 32-element head array with respect to the ultimate intrinsic SNR.
NMR in Biomedicine 23 (2):142–151.
- Levy, L. M. and A. J. Degnan (2013).
GABA-based evaluation of neurologic conditions: MR spectroscopy.
American Journal of Neuroradiology 34 (2):259–265.
- Lüdemann-Podubecká, J., K. Bösl, S. Rothhardt, G. Verheyden, and D. A. Nowak (2014).
Transcranial direct current stimulation for motor recovery of upper limb function after stroke.
Neuroscience & biobehavioral reviews 47:245–259.
- Martin, A. R., I. Aleksanderek, J. Cohen-Adad, Z. Tarmohamed, L. Tetreault, N. Smith, D. W. Cadotte, A. Crawley, H. Ginsberg, D. J. Mikulis, et al. (2016).
Translating state-of-the-art spinal cord MRI techniques to clinical use: a systematic review of clinical studies utilizing DTI, MT, MWF, MRS, and fMRI.
NeuroImage: Clinical 10:192–238.
- McRobbie, D. W., E. A. Moore, and M. J. Graves (2017).
MRI from Picture to Proton.
Cambridge university press.
- Mescher, M., H. Merkle, J. Kirsch, M. Garwood, and R. Gruetter (1998).
Simultaneous in vivo spectral editing and water suppression.
NMR in Biomedicine 11 (EPFL-ARTICLE-177509):266–272.
- Mescher, M., A. Tannus, M. Garwood, et al. (1996).
Solvent suppression using selective echo dephasing.
Journal of Magnetic Resonance, Series A 123 (2):226–229.

BIBLIOGRAPHY

Mountz, J. M., H.-G. Liu, and G. Deutsch (2003).

Neuroimaging in cerebrovascular disorders: measurement of cerebral physiology after stroke and assessment of stroke recovery.

Seminars in nuclear medicine.

Volume 33.

(1).

Elsevier,

p. 56–76.

Mullins, P. G., D. J. McGonigle, R. L. O’gorman, N. A. Puts, R. Vidyasagar, C. J. Evans, R. A. Edden, et al. (2014).

Current practice in the use of MEGA-PRESS spectroscopy for the detection of GABA.

Neuroimage 86:43–52.

Nitsche, M. A., D. Liebetanz, A. Schlitterlau, U. Henschke, K. Fricke, K. Frommann, N. Lang, S. Henning, W. Paulus, and F. Tergau (2004).

GABAergic modulation of DC stimulation-induced motor cortex excitability shifts in humans.

European Journal of Neuroscience 19 (10):2720–2726.

Provencher, S. W. (1993).

Estimation of metabolite concentrations from localized in vivo proton NMR spectra.

Magnetic resonance in medicine 30 (6):672–679.

Puts, N. A. and R. A. Edden (2012).

In vivo magnetic resonance spectroscopy of GABA: a methodological review.

Progress in nuclear magnetic resonance spectroscopy 60:29.

Ropele, S., M. Filippi, P. Valsasina, T. Korteweg, F. Barkhof, P. S. Tofts, R. Samson, D. H. Miller, and F. Fazekas (2005).

BIBLIOGRAPHY

- Assessment and correction of B1-induced errors in magnetization transfer ratio measurements.
Magnetic resonance in medicine 53 (1):134–140.
- Rothman, D. L., O. Petroff, K. L. Behar, and R. H. Mattson (1993).
Localized ^1H NMR measurements of gamma-aminobutyric acid in human brain in vivo.
Proceedings of the national academy of sciences 90 (12):5662–5666.
- Sacolick, L. I., F. Wiesinger, I. Hancu, and M. W. Vogel (2010).
B1 mapping by Bloch-Siegert shift.
Magnetic Resonance in Medicine 63 (5):1315–1322.
- Saleh, M. G., J. Near, A. Alhamud, F. Robertson, A. J. van der Kouwe, and E. M. Meintjes (2016).
Reproducibility of macromolecule suppressed GABA measurement using motion and shim navigated MEGA-SPECIAL with LCMoDel, jMRUI and GANNET.
Magnetic Resonance Materials in Physics, Biology and Medicine 29 (6):863–874.
- Saritas, E. U., J. H. Lee, and D. G. Nishimura (2011).
SNR dependence of optimal parameters for apparent diffusion coefficient measurements.
IEEE transactions on medical imaging 30 (2):424–437.
- Sclocco, R., F. Beissner, M. Bianciardi, J. R. Polimeni, and V. Napadow (2017).
Challenges and opportunities for brainstem neuroimaging with ultrahigh field MRI.
Neuroimage.
- Sherman, J. L., P. Y. Nassaux, and C. M. Citrin (1990).
Measurements of the normal cervical spinal cord on MR imaging.
American Journal of Neuroradiology 11 (2):369–372.
- Stagg, C. J., V. Bachtiar, and H. Johansen-Berg (2011).
What are we measuring with GABA magnetic resonance spectroscopy?

BIBLIOGRAPHY

- Communicative & integrative biology* 4 (5):573–575.
- Stagg, C., S. Bestmann, A. Constantinescu, L. Moreno Moreno, C. Allman, R. Meke, M. Woolrich, J. Near, H. Johansen-Berg, and J. Rothwell (2011).
Relationship between physiological measures of excitability and levels of glutamate and GABA in the human motor cortex.
The Journal of physiology 589 (23):5845–5855.
- Stroman, P., B. Tomanek, V. Krause, U. Frankenstein, and K. Malisza (2002).
Mapping of neuronal function in the healthy and injured human spinal cord with spinal fMRI.
Neuroimage 17 (4):1854–1860.
- Tremblay, S., V. Beaulé, S. Proulx, L. De Beaumont, M. Marjańska, J. Doyon, A. Pascual-Leone, M. Lassonde, and H. Théoret (2012).
Relationship between transcranial magnetic stimulation measures of intracortical inhibition and spectroscopy measures of GABA and glutamate+ glutamine.
Journal of neurophysiology 109 (5):1343–1349.
- Van Gelderen, P., J. De Zwart, P. Starewicz, R. Hinks, and J. Duyn (2007).
Real-time shimming to compensate for respiration-induced B0 fluctuations.
Magnetic Resonance in Medicine 57 (2):362–368.
- Wolff, J., F. Joo, and P. Kasa (1993).
Modulation by GABA of neuroplasticity in the central and peripheral nervous system.
Neurochemical research 18 (4):453–461.